REPUBLIC OF IRAQ

MINISTRY OF HIGHER EDUCATION AND SCIENTIFIC RESEARCH

BABYLON UNIVERSITY

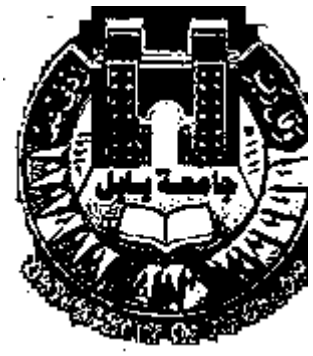

A STUDY OF STATIC AND DYNAMIC STATE OBSERVER APPLIED TO AN INDUCTION FURNACE

A THESIS SUBMITTED TO

BABYLON UNIVERSITY,

COLLEGE OF ENGINEERING

IN PARTIAL FULFILLMENT OF THE REQUIREMENTS FOR THE DEGREE OF MASTER OF SCIENCE IN MECHANICAL ENGINEERING

(Applied Mechanics)

By:

HAZIM WALLY CHILLAB

B.Sc. 2005

2009

جمهورية العراق
وزارة التعليم العالي والبحث العلمي
جامعة بابل

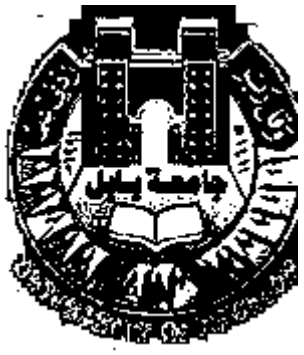

دراسة
مخمّني حالة ستاتيكي و ديناميكي
وتطبيقهما على أفران الحث الكهربائي

أطروحة مقدمة إلى
جامعة بابل، كلية الهندسة
كجزء من متطلبات نيل درجة الماجستير في علوم الهندسة الميكانيكية
(الميكانيك التطبيقي)

اعداد

حازم والي چلاب

B.Sc. 2005

2009

1.1 GENERAL VIEW:

The advancement of any nation technologically has been influenced and elevated by the extent to which it can usefully harness and convert its mineral resources, and by its utilizing energy efficiently. The productions of metal in foundries and in all human lives have also become a general practice. Different melting techniques have been known with different energy sources. While electricity is being used in about all applications, the search of increasing its efficiency is taking a lot of attention.

One of the most electrical furnaces used is the induction furnaces, because of its many advantages such as: fast start up, flexibility, natural stirring action, clean melting, safe automatic operation, compact installation, better working environment, energy conservation, and decreased costs.

Although melting process seems a simple process, but in fact it is a difficult and complicated one, and one of these difficulties is the charge temperature, which is unmeasurable because of the severe conditions with high temperatures.

The present work use state estimation technique in both types, static and dynamic, in order to assign the temperature of induction furnace charge based on the measurements from the furnace system and the statistical properties of both the measurements and the noise.

Static state estimator (observer) is used based on the WLS approach assuming there are four thermocouples in the insulation layer. While, dynamic

state observer is used the MMAE technique based on three adaptive Kalman filters assuming there is a single thermocouple in the furnace lining .

1.1.1 INDUCTION FURNACES:

Electromagnetic induction, or simply induction is a way to heat electrically conductive materials, such as metals. It is commonly used in process heating prior to metal working, and in heat treating, welding, and melting. Induction heating relies on electrical currents that are induced internally in the workpiece material. These so called eddy currents causing heat.

The first induction furnace for melting metal was made by Kjellin in 1900, which was a ring type furnace. But for commercial use, the first induction furnace developed by Northrup in 1917, which used frequencies higher than normal value which is 50 Hz [1]. The Ajax Electrothermic Co. of America did much of the commercial development work on these furnaces. In 1930 the Gillette Razor Co. of America [1] installed a plant for the induction hardening of razor blade strip. The next major application of induction heating seems to have been in 1936 to the surface hardening of the bearing surfaces of crank shafts for the motor industry [1].

Induction melting is widely used in the production of iron and steel castings and for melting aluminum, zinc, copper, and a great variety of other

nonferrous alloys. In very general terms, an induction melting furnace can be defined as an apparatus that induces an electric current in the electrical conducting charge material to be melted. This is done by electromagnetically coupling the charge with the coil carrying an alternating current. The current in the coil induces eddy currents in the charge which heats and melts the metal.

The most two common induction melting furnaces designs are the coreless furnace and the channel furnace [2]. In the coreless furnace, also called crucible furnace, Fig. (1.1), the crucible made of refractory material that contains the metal. A water-cooled power coil surrounds this crucible and a number of magnetic yokes which concentrate the magnetic field established by the coil current. These yokes also eliminate the generation of a high magnetic scatter field and heating up of the furnace structure, figures (1.2) and (1.3). The power coil carries a large electric current which establishes an alternating magnetic field. The field induces eddy currents in the metal bath, this eddy currents affect resistance heating of the bath.

There is always an ideal relationship between the size of a coreless furnace and its operating frequency. As a general rule, a small furnace gives best results at high to medium frequencies and large furnaces work best at the lower frequencies.

The current density of the induced eddy current is highest in the refractory crucible and the surface of the metal batch and decreases to zero in

the centre of the melt. This effect is generally known as skin effect. The penetration depth and the bath movement increase with lower frequency while the energy input increases with higher frequency. Depending on the application, induction furnaces are used as medium frequency furnaces with a frequency ranging from 110 to 1,000 Hz.

The eddy currents also cause a bath movement in the furnace that decreases with increasing frequency. This bath movement is a characteristic for crucible induction furnaces. It ensures effective stirring of the bath with the resulting homogeneity of the melt. Well-designed crucible induction furnaces have the coil system separated into an upper section and a lower section. Depending on the actual melt condition and the degree of filling of the furnace, power can be directed to the lower or to the upper section of the coil system. The so called “power-focus-technology” permits optimal usage of the furnace power.

Crucible induction furnaces are particularly attractive for melting charges and alloys of known analysis; in essence, the operation becomes one of metal melting with rapidly absorbed electric heat without disturbing the metallurgical properties of the initial charge.

The efficiency of crucible induction furnaces is in the range of 60 to 70 %. The crucible induction furnace is ideally suited to melt scrap with high specific surface area since there is no contact with combustion products [3].

Figure (1.1): Coreless induction furnace

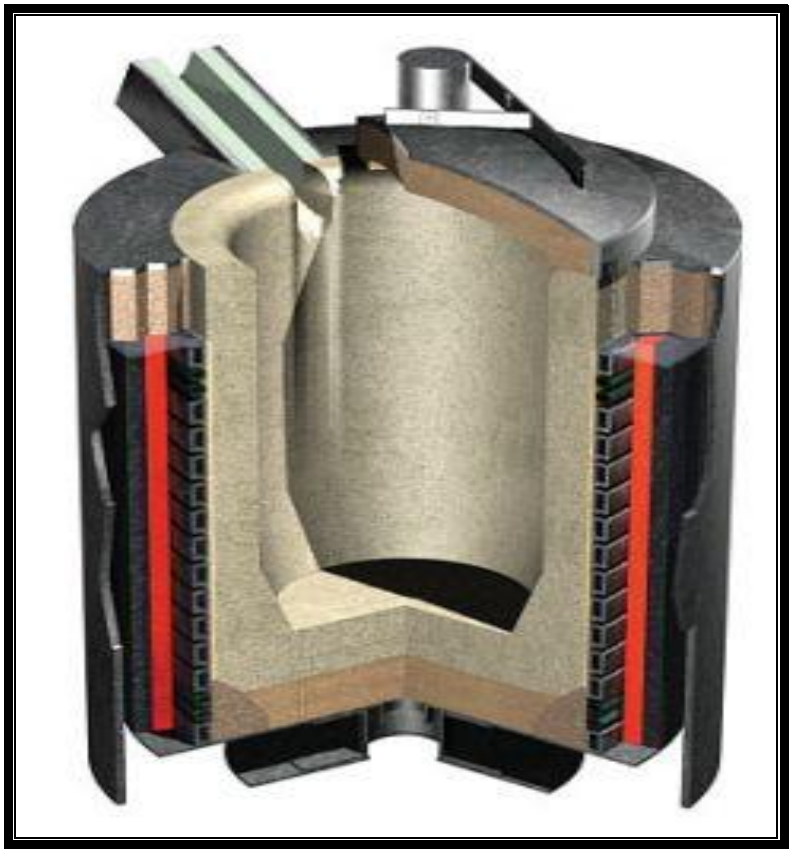

Figure (1.2): Structure of crucible induction furnace

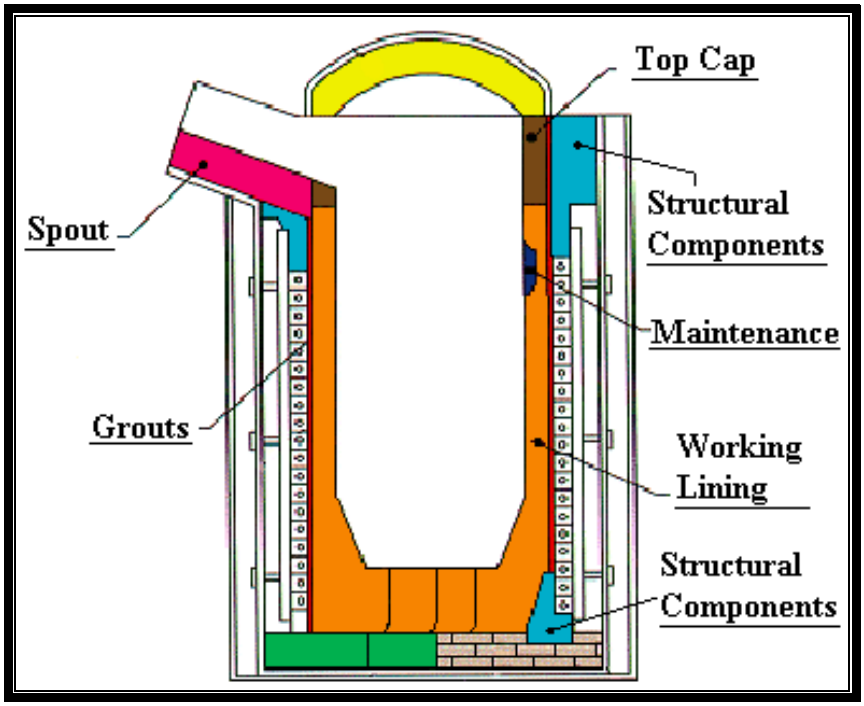

Figure (1.3): Structure of crucible induction furnace

In the cored type, also called channel induction furnace, Fig. (1.4), the principle of heat generation is comparable to that of a transformer. It is actually wound to conform to a typical transformer design having an iron core and layers of wire acting as primary circuit. The melting channel acts as a ring short circuit around this transformer in the melting chamber. According to the desired melting capacity, one, two or even more such transformers (or inductors as they are called) may be added to the furnace shell. At all times, the channel must hold sufficient metal to maintain a short circuit around the transformer core. Air-cooling is used as required to prevent excessive heating of the inductor coils and the magnetic cores.

The core-type furnace is the most efficient type of induction furnace because its iron core concentrates magnetic flux in the area of the magnetic

loop, ensuring maximum power transfer from primary to secondary, efficiency in the use of power can be as high as 95 to 98 % [3].

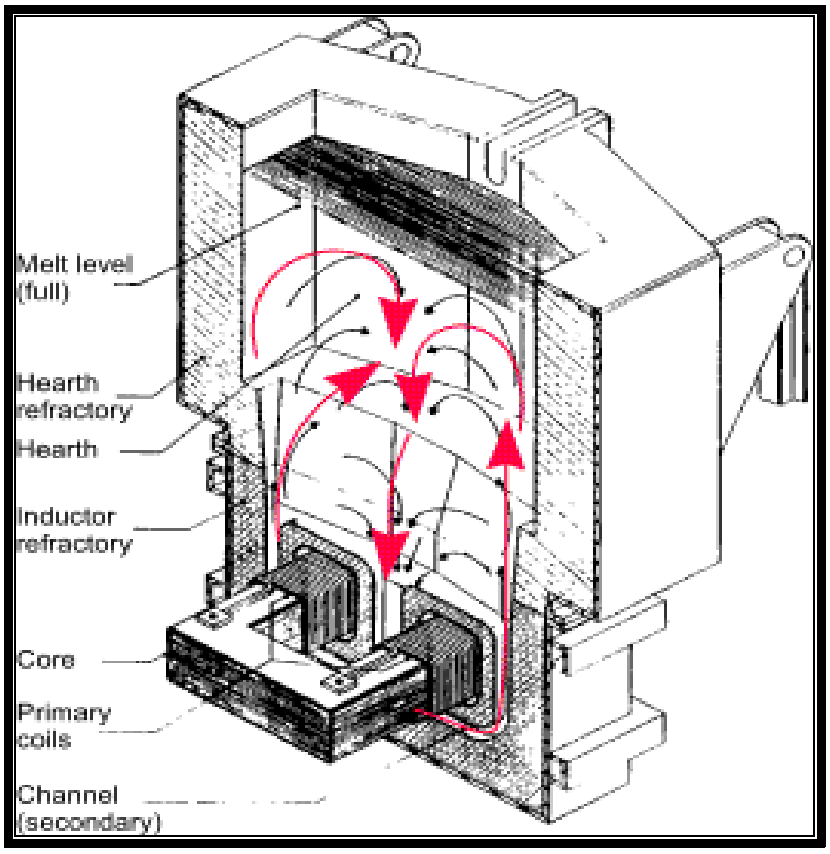

Figure (1.4): Channel induction furnace

1.1.2 MELTING PROCESSORS:

The invention of computers has revolutionized nearly all branches of engineering. They are widely used in design, analysis, manufacturing, process and industrial control, data collection and processing, and other numerous areas. Personal computers (PC) are used in feedback control of processes and in data acquisition. Digital signal processing and intelligent instrumentation for error corrections are also used.

Control and data acquisition systems are used for industrial and process control or with test equipment. In process control packages a virtual user interface may be used, which looks like a control panel with push buttons, warning lights, trending graphs, etc., but is operated with a mouse [4].

For melting, the charge temperature continuously measured and sent to the computer for analysis and display. The computer calculates the mean temperature of the charge on the basis of the furnace content and the input energy. After melting down the computer prompt the operator to measure the temperature which is taken over the place of the calculated temperature. At this stage the computer calculates the energy necessary to raise the temperature of the melt to the pouring temperature. Once this energy is consumed, the computer switch the furnace power supply off.

1.1.3 TEMPERATURE MEASUREMENTS:

The temperature measurements have a great importance in many industrial melting process, as a control parameter. It does not matter whether the temperature measurement instruments are simple thermocouples or the latest products of advanced technology, however, its performance is a critical factor in the production of accurate data.

Some of the commonly used and the recently developed transducers are described below:

1. *Thermocouples*:

The general principle is that when two materials are connected to each other in a junction and they are both connected to a voltmeter, then if the junction is heated, the meter should show a voltage. This is known as the thermocouple effect. It is part of a broader picture since in an electrical conductor a difference of temperature is associated with a difference of electric potential. The potential varies in different materials.

It is a very good and wide ranging instrument because of its simplicity, cheapness, and the wide range of temperature works in it depending on the materials used for making the junction of the thermocouple, such as chromel/ alumel type up to 1000 ^{o}C , iron/ constantan which is recommended for only 800 ^{o}C, and platinum based couples [4].

In industry, it is not usual to run the thermocouple itself to a distant instrument but to use an extension cable. This may also apply if a transmitter is used but has to be kept away from hot equipment. Extension cable is made of the same material as the couple but with tougher insulation, and possibly thicker wire for lower resistance.

There is some limitations in using thermocouples due to:

a. The possibility of melting the thermocouple at the high temperature environments.

b. Peltier effect, which heats or cools the junction when a current flows through the couple.
c. Thomson effect, which is heating or cooling along the wires as the current flows in the wires with or against the temperature gradient.

In addition to these general limitations, there are two main problems when using thermocouples to measure the temperature of the insulator or any other part of induction furnaces, which are:

a. Eddy currents will be generated inside the thermocouple.
b. High frequencies produced electromagnetic waves which cause the measurements to be noisy.

2. *Radiation Pyrometers*:

They have some advantages for measuring surface and furnace wall temperature because they can be used for remote monitoring. But it has certain disadvantages like it requires knowledge of the emittance of the surface to be measured, because due to inaccurate values of emittance errors showed up in the measurements, but the major limitation is the high cost of such units [5].

3. Optical fiber system:

The use of optical fiber system as a means of temperature control has been established for both contact and non-contact measurements. Essentially the system consist of a fiber optic bundle of glass or sapphire. The fibers are sensitive only to the infra-red portion of the spectrum and

filter out the other radiation. Since they are relatively inert at high temperatures, they can be operated without the need to be cooled.

The fibers have been used as probes for continuous measurement of molten metal temperature. The operation done by inserting the fibers beneath the metal surface and continuously keeping the feeding to compensate the erosion of the fibers tips.

As a means of the continuous temperature measurement, the optical fiber system has considerable potential, but the very high cost of such units limits the applications of using it in a wide range.

4. Resistance thermometers:

The most usual resistance thermometers use platinum against one of two platinum/rhodium alloys. The metals may be of very fine wires wound on a ceramic carrier, secured locally with a refractory cement, or deposited on a non-conducting base as thin films; another form is helical coils loosely held in a multi-bore alumina tube. The active bulb is typically 25 mm long, including the filament carrier and immediate protection.

In some versions the protection have small holes to allow circulation for better thermal contact with the medium being measured.

1.2 STATE ESTIMATION:

State observer is an approach that is used to estimate the state of a system based on available measured data, or the process that assigning

values to an unknown system state or parameters based upon the noise-corrupted observation involving some functions of the state or the parameter [6].

It is assumed that both the states and the unwanted noise have known statistical properties. The value assigned is called the estimate, and the system or the function that yield the estimate is called the observer. State observer is either static or dynamic. Figure (1.5) shows the structure of a control system with an artificial observer. In the problem under study, the plant is an induction furnace.

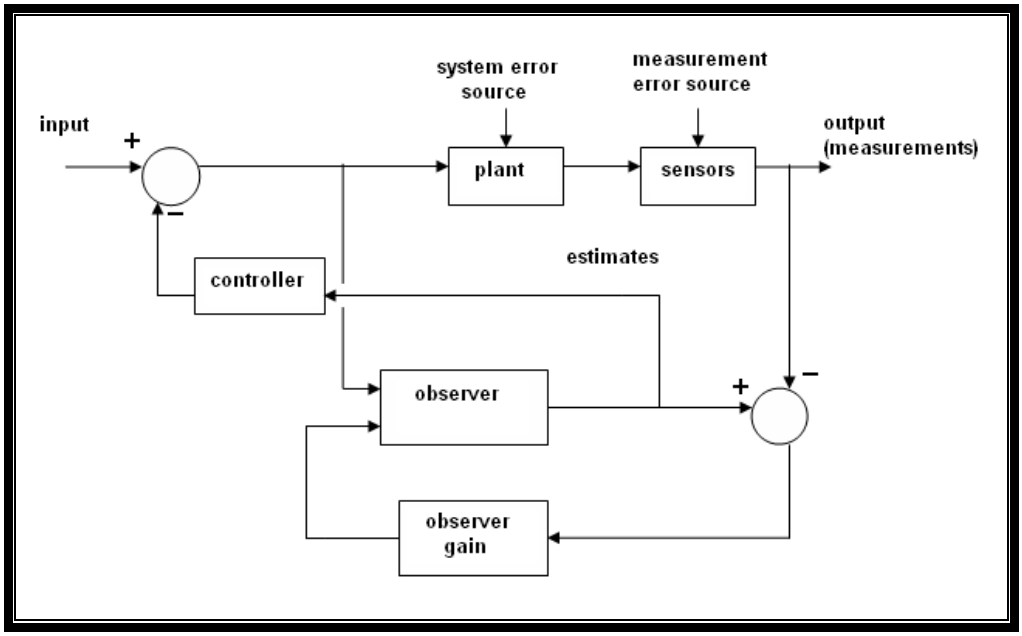

Figure (1.5): Control system with an observer [6]

1.3 FURNACE DESCRIPTION:

The induction furnace consists basically of a crucible, inductor coil, shell, cooling system and tilting mechanism. The crucible is formed from

refractory material, which the furnace coils is lined with. This crucible holds the charge material and subsequently the melt. The choice of refractory material depends on the type of charge, i.e. acidic, basic or neutral. In this design a neutral refractory is used which made of zirconium oxide (ZrO_2).

The furnace design analysis is based on a half ton capacity [7]. The shape of the crucible is cylindrical. The internal diameter of the crucible is taken as 40 cm, while the height of the melt is taken as 60 cm. The thickness of the refractory lining is taken equal to 6 cm.

The inductor coil is a tubular copper coil with specific number of turns equal to ten turns. A 5000 Ampere alternating current (A.C) with 500 Hertz frequency passes through the coil.

The cooling system is a through-one-way- flow system with the tubular copper coils connected to water source with 298 Kelvin at the inlet.

1.4 OBJECTIVE OF THE WORK:

The present work is concerned with estimating the charge temperature of a coreless induction furnace of a half ton capacity, depending on a software instead of hardware in order to:

1- Increasing the measurement redundancy.

2- Decreasing the error in the estimating process.

2.1 LITERATURE REVIEW:

Baker [8] referred to the analytical solution of classical heat flow problem as a method of analyzing the more practical heat flow problems of induction heating.

The solution of a long cylinder is given, initially at zero temperature, supplied with constant power at the surface, starting at time equal to zero. Theoretical results are favorably compared with the experimental results, and presented in a dimensionless form.

Schweppe et al. [9] in a three parts series, a static state estimator is developed, where in the first part the general problem, model, and theory of solution are developed, in the second approximate models and solutions are developed, while in the third consideration is given to implementation problems related to computational speed, dimensionality of the state vector, and the fact that a power system is never truly in steady state. The used technique is a weighted least square approach for an off-line application.

Dopazo et al. [10] describes a method for computing a real-time load flow of a power system. The use of line flow measurements is proposed and it is shown that this measurement scheme shows superiority in speed, accuracy and numerical behavior together with advantages in error detection and identification. The proposed measurement scheme yields a set of compatible data which satisfies economic considerations as well as the requirements to obtain an acceptable solution in the event of outages of the metering system.

The computational process is very stable and has excellent convergence characteristics. Differences between measured and estimated values for both measured and non-measured line flows were found to be within the error bounds used for the measured quantities.

Lenden et al. [11] presented a comparison between three different methods for determining the thermal diffusivity of a long copper rod as an example of one dimensional heat diffusion process.

The methods used are modified Angstrom's method, least square method, and maximum likelihood method, which have been applied to data obtained from experiments on a long copper bar.

The comparison based on the accuracy, the amount of computation, the storage capacity, and in general the advantages and the limitations of each method. The results showed that the maximum likelihood method provides greater accuracy but more computational time and storage than the other methods.

Lausterer et al. [12] used a parameter state estimation to estimate the radial and axial temperature distribution of a stainless steel cylindrical ingot being heated in three zone furnace.

The Kalman filter he used was rapidly convergent even in cases of high measurements noise, and few sensors. It is concluded that even when the estimation algorithm is not run in a real time, it gives a robust estimation.

Soderstrom et al. [13] has analyzed and compared five different identification methods which are the least squares method, the instrumental variables method, the generalized least squares method, the extended least squares method, and the maximum likelihood method.

These methods are examined from a theoretical viewpoint. The possibilities of convergence and simulation studies indicate that the greater accuracy is for the maximum likelihood method.

Tysso [14] described an adaptive control system for a ship boiler. The model developed of a simple form with few characteristic parameters and it depends on an extended Kalman filter approach. The model worked satisfactorily for the whole range of operation and the transient behavior caused by a sudden change properly described.

Xiang Nian-de et al. [15]presents an approach for detection and identification of multiple bad data, estimation-identification approach which has been developed in order to improve the performance of static-state estimators of power systems, this approach is based upon the residual sensitivity matrix.

The detection and identification of all bad data found in one computation run, also, the state variables and the measurement are estimated efficiently even when gross errors exist in the measurements.

Mili et al. [16] provides a comparative assessment of the identification methods, these methods are first classified, then explored and compared.

Three broad classes are distinguished : the class of identification by elimination (IBE), the class of the non-quadratic criteria (NQC), and the hypothesis testing identification (HTI).

The investigations are based upon both theoretical and practical considerations, where Five criteria are selected for assessing the quality of the various identification methods. The first three of them are the main objectives sought by any identification approach as such, the two others concern its practical feasibility, i.e. the applicability requirements. these criteria are ability to localize exactly the bad data, the aptitude for clearing the final data base, recognition of topologically unidentifiable bad data, implementation requirements, and computing time.

The study shows that the NQC techniques exhibit the most poor performances, and they have a slow convergence, in brief, they don't show to be suitable enough. On the other hand, the IBE techniques are attractive with respect to implementation considerations, they are easy to use and simple to implement. While the HTI method seems to combine effectiveness, reliability and compatibility with on-line implementation requirements.

Stavros et al. [17] developed a microprocessor system in laboratory, to measure the thermophysical events taking place in furnaces, but also to control the furnace.

The induction furnace control system measures the temperature of the specimen inside the coil. The control thermocouple was inserted in a small

groove at the specimen's edge. The other thermocouple was located in the specimen's center.

A constant linear heating rate applied at the specimen's edge with the measurement of the temperature of both the edge and the center. When the edge reaches the given temperature, the controller keeps the temperature constant.

The thermocouple was exposed to corrosive attack and then destroyed at high temperature.

Another melting processor was mentioned, it was proposed by ABB (Asia Brown Boveri), the system consists of a personal computer, with a graphical representation of the melting process to provide the operator with the necessary information and to allow interaction with the process.

Potapov et al. [18] presented a theoretical modeling of the process of heating of a solid round billet in an induction furnace in order to develop optimum heating ensuring a minimum temperature difference over the cross-section of the billet. The heat flow assumed to be only in radial direction. Results of the calculations were in good agreement with the experimental data.

Liete et al. [19] presents a comparison between the performance of dynamic and tracking estimators, in power systems operating under quasi-static conditions, concerning their characteristics of forecasting and filtering,

in order to know the main advantages of both algorithms. Based on these knowledge a new dynamic estimator is built. The proposed dynamic state estimation algorithm is tested with a power system operating under normal and abnormal conditions, the results showed that the estimator works efficiently.

Al-Ubaidy [6] had used the state estimation technique in order to predict the temperature of an induction furnace charge. A finite element software package was used. The numerical results are favorably compared with the analytical results obtained by Baker [8]. In the technique which was used the model was depending on a five elements state vector with a measurement redundancy equal to two. The results showed a good accuracy.

Jifeng et al. [20] proposed an approach to detect, identify, and estimate failures, including abrupt total, partial, and multiple failures, in a dynamic system. The new approach, named IM^{3}L, is developed based on variable-structure multiple-model estimation, which allows to improve performance by online adaptation. It uses an interacting multiple model estimator for fault detection and identification but the maximum likelihood estimator for estimating the extent of failure. It provides an effective and integrated framework for fault detection, identification, and state estimation. the proposed approach is evaluated and compared

with multiple-model approaches and a widely used single-model residual-based generalized likelihood ratio approach in terms of detection and

estimation performance. The results show that the IM^3L provides not only fast detection and proper identification,

but also good estimation of the failure extent as well as robust state estimation.

2.2 LITERATURE SUMMARY:

State estimation and statistical filtering have been used in many applications throughout the last fifty years, in order to eliminate or to reduce errors, or to assigning values for the unmeasurable parameters, that's why it takes a lot of interest from many researchers.

Although there are different methods and algorithms, but there is a kind of consensus on the least squares method and the Kalman filter technique because of their simplicity, rapid convergence, and the good agreement with the real values, that's why many approaches based on them, and for that the present work will be depending on them.

3.1 INTRODUCTION :

Induction heating is a relatively recent process heating method, introduced commercially about 90 years ago. The main utilization of induction heating technology centers around its unique properties that distinguished it from other heating technologies, such as quick heating, fast start up, energy saving, and high production rates.

The main property is the skin-effect phenomenon which happened when the eddy current induced in the workpiece, it concentrates near the surface. This phenomenon creates a heating source in the metal surface itself. So the result is a heating method requiring no external heating but using the piece to be heated as its own heat source. The method also requires no physical contact with the energy source or the induction coil. Further property is the ability to select the heated depth by the choice of frequency.

3.2 POWER GENERATION:

The coil and the current distribution for the induction furnace are shown in figure (3.1). A high alternating magnetic field has been produced in the work coil which induces eddy currents within the metal. The eddy currents causes resistance to their flow and the metal is heated. The current decays nearly exponentially from the surface to the center of the work piece [21].

The penetration depth which is the depth of the equivalent direct

current and is defined as the depth at which the current density is 36.7 percent of its surface value, which is given by [22]:

$$\delta = 50 \cdot 3\sqrt{\frac{\rho_e}{f\mu_r}} \qquad \ldots (3.1)$$

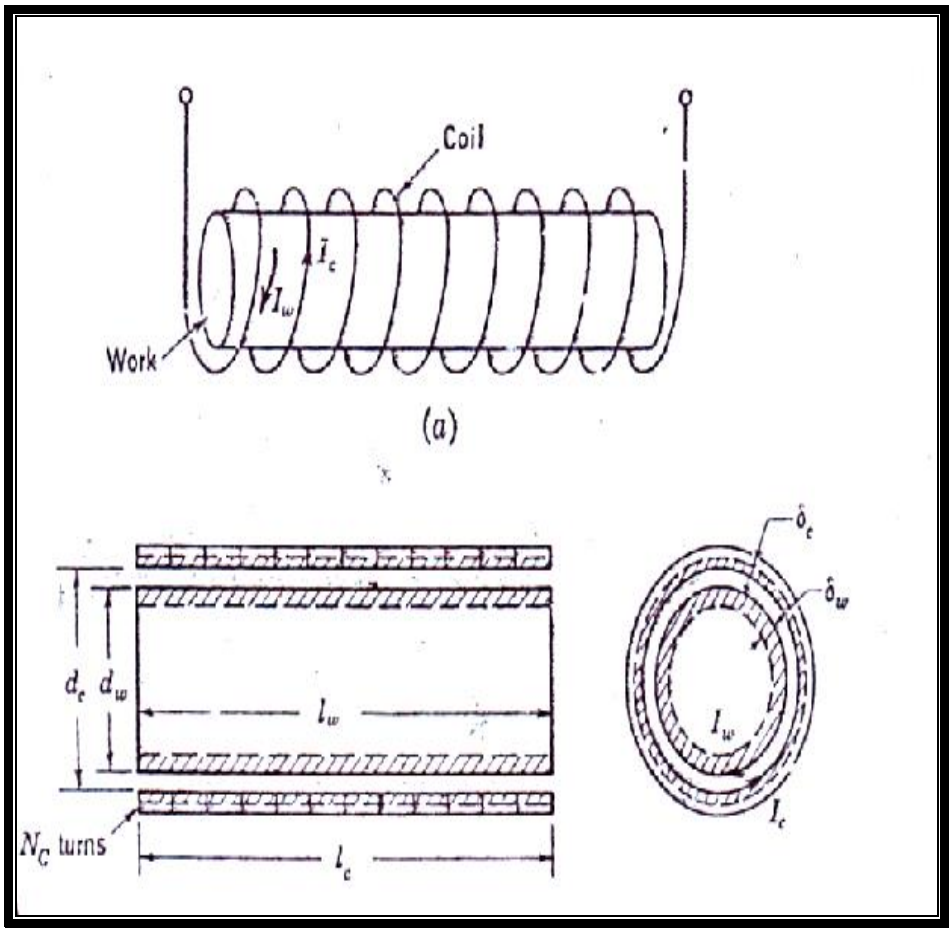

Figure (3.1):Current depth in an ideal workpiece [21]

About ninety percent of the total generated heat is being generated in the surface layer of thickness δ [3]. Obviously the layer is thinner for high frequency currents, Fig. (3.2), and it is more efficient but requires longer heating time in order to conduct to the center.

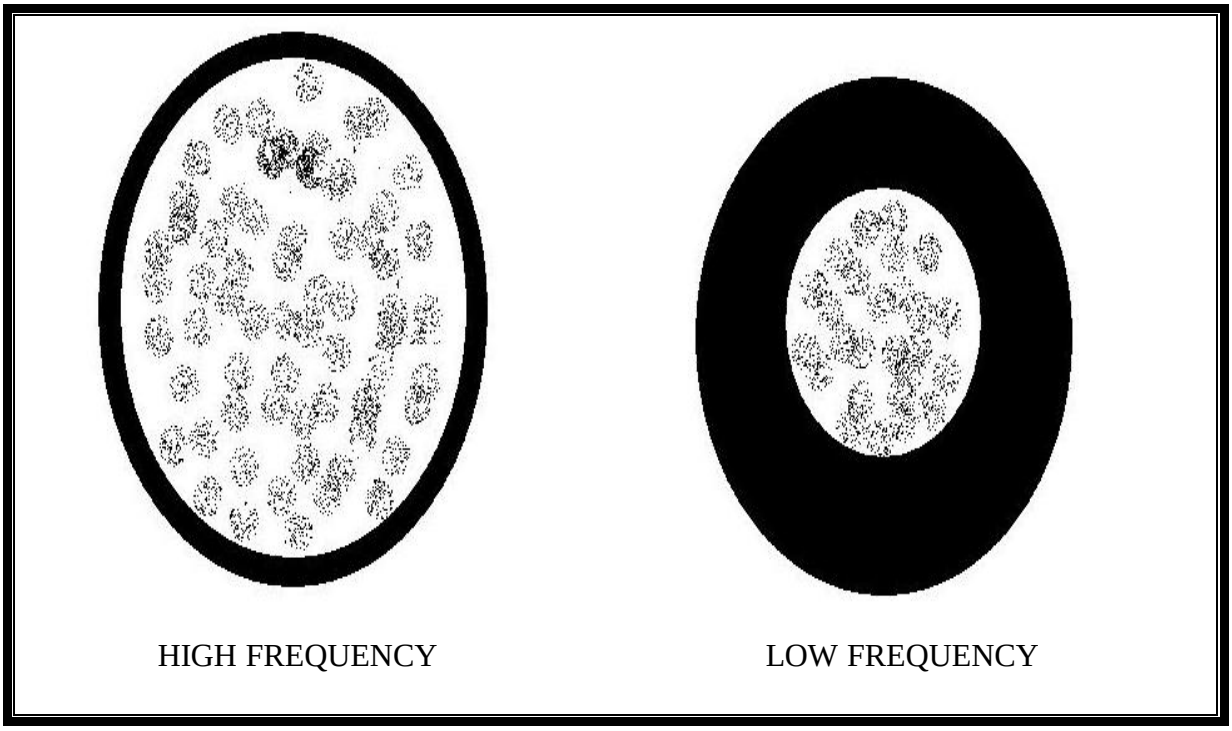

Figure (3.2): Effect of frequency on current penetration

Since induction depends on the magnetic properties of the workpiece, so it is important to pay attention for those properties. One of the most important properties is the permeability which is the unitless measure of flux density in the material divided by what the density would have been in air [22], or simply it is a measure of how magnetic a material is.

Most materials can be divided into three magnetic classifications. The first group is paramagnetic and has permeability slightly greater than unity, for example aluminum and platinum. The second group, classified as ferromagnetic which contains three metals, iron, nickel, and cobalt, which have magnetic permeability value many times greater than unity. The third group, called diamagnetic which has permeability slightly less than unity, such as copper, gold, and bismuth. For the purpose of induction heating all

materials are said to have unity permeability except of course the ferromagnetic group. For iron the permeability is given by [21]:

$$\mu_r = 1 + \frac{32400}{H_o} \quad \ldots (3.2)$$

Where, H_o is the magnetic flux intensity which is given by [7]:

$$H_o = \frac{I_c \cdot no}{l_c}$$

The case of ferromagnetic material is further complicated than the other materials, this is because in induction heating the surface may rise above the Curie point, which is the point at which the ferromagnetic materials lose their magnetic properties and their permeability suddenly drop to unity, before the rest of the work piece. The fact that the power input is proportional to permeability indicates that the surface power input or heating rate will decrease as the Curie point is reached. At some point from the surface, the temperature will be still below the Curie point, the material will be magnetic, and the flux will be at a maximum. The flux increases from the center towards the surface and concentrates at the most magnetic cross-sections.

3.3 CHARGE TEMPERATURE RISE MODELING:

The exact analytical solution to the problem of transient temperature variation in materials, for two dimensional case is complex, because it

requires the solution of system of partial differential equations. This type of solution is inappropriate for on-line computer applications.

For practical monitoring applications, the thermal system can be approximately represented as a lumped system described by ordinary differential equations, which are much easier and faster to solve numerically.

The lumped thermal model assumes that the heat storage in a material can be represented by an effective thermal capacitance, C, and that the resistance to the heat flow between two points can be represented by an effective thermal resistance, R. Electrical analogy can be used in this case, in which current represents heat flow and voltage represents temperature. Figure (3.3) illustrates a circuit model for determining the temperature, T, at a point in an object (charge, insulation, ...etc.) given the heat, q_i, flowing through or generated at that point.

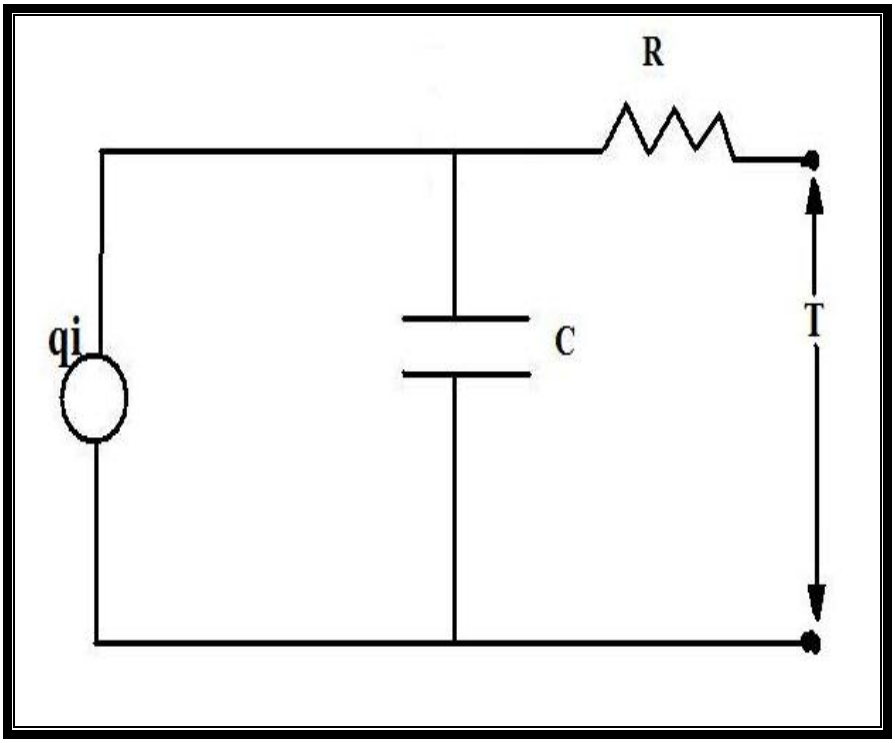

Figure (3.3): Representation of a node in the charge

The lumped model approach results in first-order dynamics in the temperature response to the heat input at a given point, or node. For the single node illustrated in Fig. (3.3), after certain linearization the heat balance equation is simply given by [23]:

$$q_i = \frac{T(t) - T_a(t)}{R} + C\frac{dT(t)}{dt} \qquad \ldots (3.3)$$

Where q_i is the power generated at node i. This equation may be put in state variable form, anticipating the construction of a set of dynamic equations for describing temperature distribution in the chargé of an induction furnace:

$$\dot{T} = \frac{(T_a - T)}{R.C} + \frac{q_i}{C} \qquad \ldots (3.4)$$

3.3.1 HEAT GENERATION IN A NODE:

The induced power generation inside the cylindrical charge of an induction furnace varies along the radius, its variation is approximately exponential. To obtain a set of linear differential equations for the lumped parameter model, q_i is assumed to be equal to the total heat generated for the particular node described by Eq. (3.3), which derived by considering the total current flowing in a shell of thickness δ_r and a work length of unity, figure (3.1), which is [21]:

$$I_{tr} = I_r \cdot \delta_r \qquad \ldots (3.5)$$

where I_r is the current density at a shell of radius r, which is given by [21]:

$$I_r = -\frac{A \cdot k}{4\pi}(ber'(kr) + bei'(kr)) \qquad \ldots (3.6)$$

Where,

$k = \sqrt{\frac{8\pi^2 f \mu_r}{\rho_e}}$, and

A, is a constant which is given by [21]:

$$|A|^2 = \frac{H_o^2}{(ber^2(kr_c) + bei^2(kr_c))}$$

ber(x) and bei(x) are the modified Bessel functions (Kelvin functions) which are numerically given as:

$$ber(x) = \frac{e^{x/\sqrt{2}}}{\sqrt{2\pi x}}(\sin(\frac{x}{\sqrt{2}} + \frac{3\pi}{8}) + \frac{1}{8x}\sin(\frac{x}{\sqrt{2}} + \frac{\pi}{8}))$$, and

$$bei(x) = \frac{e^{x/\sqrt{2}}}{\sqrt{2\pi x}}(\sin(\frac{x}{\sqrt{2}} - \frac{\pi}{8}) + \frac{1}{8x}\sin(\frac{x}{\sqrt{2}} - \frac{3\pi}{8}))$$

The charge material resists the current flow, this resistance is given as [21]:

$$R_r = \frac{2\pi\rho_e r}{\delta_r} \quad \ldots (3.7)$$

Due to this current flow resistance the heat is dissipated inside the charge. This power could be computed as:

$$I_{tr}^2 R_r = 2\pi\rho_e r\delta_r \cdot I_r^2 \quad \ldots (3.8)$$

Integrating Eq. (3.8) from inner radius r_i to outer radius r_o i.e.,

$$q_i \Big/ (\frac{|A|^2 k^2 \rho_e}{8\pi^2}) = \int_{r_i}^{r_o} r[(ber'(kr))^2 + (bei'(kr))^2]dr$$

$$= \left[\frac{r}{k}\{ber(kr)ber'(kr) + bei(kr)bei'(kr)\}\right]_{r_i}^{r_o}$$

$$= \frac{1}{k}[r_o\{ber(kr_o)ber'(kr_o) + bei(kr_o)bei'(kr_o)\} - r_i\{ber(kr_i)ber'(kr_i) + bei(kr_i)bei'(kr_i)\}] \quad \ldots (3.9)$$

Simplifying Eq. (3.9) will take the following form for a length of Δz:

$$q_i = 2.5 f H_o^2 \Delta z \mu_r \pi r_c Q_n * 10^{-2} \quad \ldots (3.10)$$

Where,

$$Q_n = \frac{2}{ka}\frac{AA - BB}{CC}$$,

$$AA = r_o\{ber(kr_o)ber'(kr_o) + bei(kr_o)bei'(kr_o)\}$$,

$$BB = r_i\{ber(kr_i)ber'(kr_i) + bei(kr_i)bei'(kr_i)\}$$,

$$CC = ber^2(kr_c) + bei^2(kr_c)$$,

3.4 FURNACE DYNAMIC THERMAL MODEL:

Figure (3.4) shows one way in which the basic thermal network may be set on for a charge in a furnace. The charge is assumed to be insulated all around and heat will escape through the insulator (in radial direction) towards the cooling water by virtue of temperature difference.

Following the approach represented by Eq. (3.4), the temperature dynamic equation for any node (node m,k) of the furnace charge can be written as:

$$\dot{T}_{m,k} = \frac{1}{C_{m,k} \cdot R_{m+1,k}}(T_{m+1,k} - T_{m,k}) + \frac{1}{C_{m,k} \cdot R_{m-1,k}}(T_{m-1,k} - T_{m,k}) + \frac{1}{C_{m,k} \cdot R_{m,k+1}}(T_{m,k+1} - T_{m,k}) + \frac{1}{C_{m,k} \cdot R_{m,k-1}}(T_{m,k-1} - T_{m,k}) + \frac{q_m}{C_{m,k}} \quad \ldots (3.11)$$

Where,

$$C_{m,k} = \rho_{m,k} C_{p_{m,k}} \Delta V_{m,k},$$

$$\Delta V_{m,k} = r_m \Delta r \Delta \phi \Delta z,$$

$$R_{m+1,k} = \frac{\Delta r}{(r_m + \Delta r/2)\Delta \phi \Delta z k_c},$$

$$R_{m-1,k} = \frac{\Delta r}{(r_m - \Delta r/2)\Delta \phi \Delta z k_c},$$

$$R_{m,k+1} = \frac{\Delta z}{r_m \Delta \phi \Delta r k_c},$$

$$R_{m,k-1} = \frac{\Delta z}{r_m \Delta \phi \Delta r k_c},$$

And $q_m = q_i$ as given by Eq. (3.10).

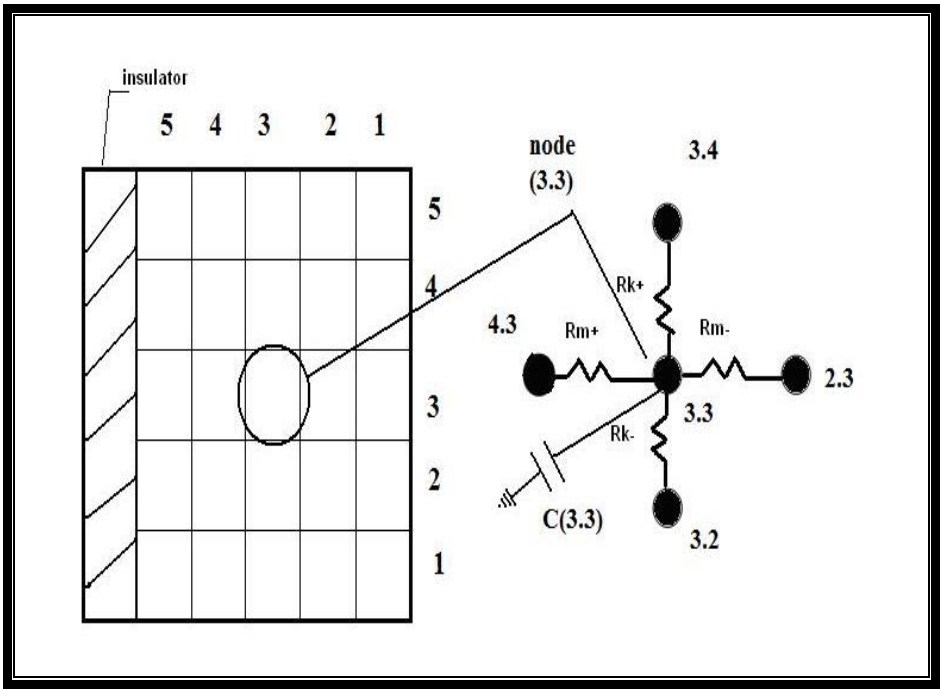

Figure (3.4): Equivalent R-C simulation of the charge

Writing Eq. (3.11) for each of the specified nodes leads to a system of first order dynamic equations. This set of equations are solved by using fourth-order Runge-Kutta method. Figure (3.5) shows the flow chart of the main program used in analyzing an induction furnace dynamics.

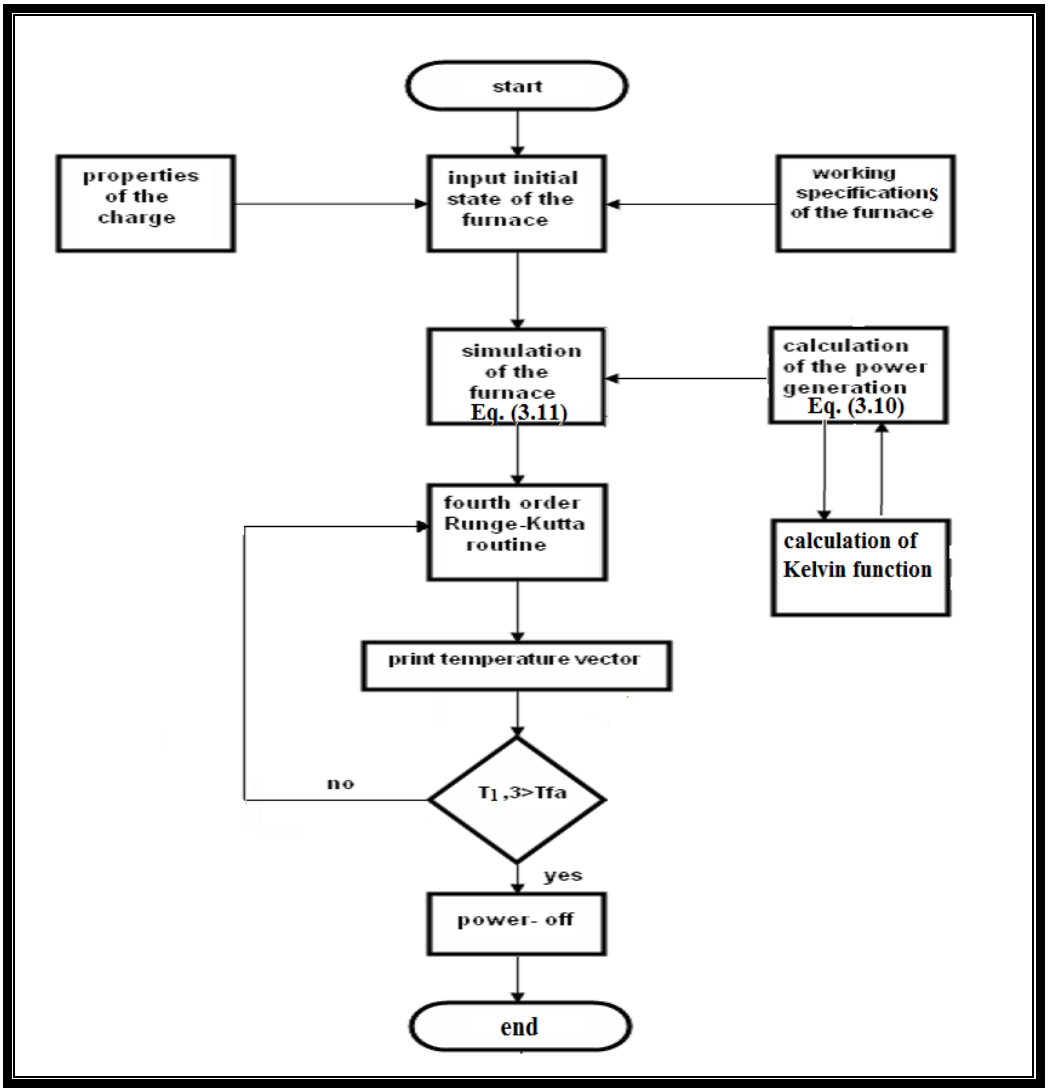

Figure (3.5): Flow chart of the furnace dynamic simulation

3.5 COMPUTATIONAL RESULTS :

For the purpose of checking the theoretical model of the melting process of a solid cylindrical charge in the induction furnace, the charge is divided into five rings in the radial direction and five sections in lengthwise direction. Hence using the geometrical parameters of the furnace, $\Delta z=0.12m$, $\Delta r =0.04m$, and $\Delta\varphi =2\pi$ (symmetric), figure (3.6).

A set of runs were made in order to check the model validity and analyze the furnace performance.

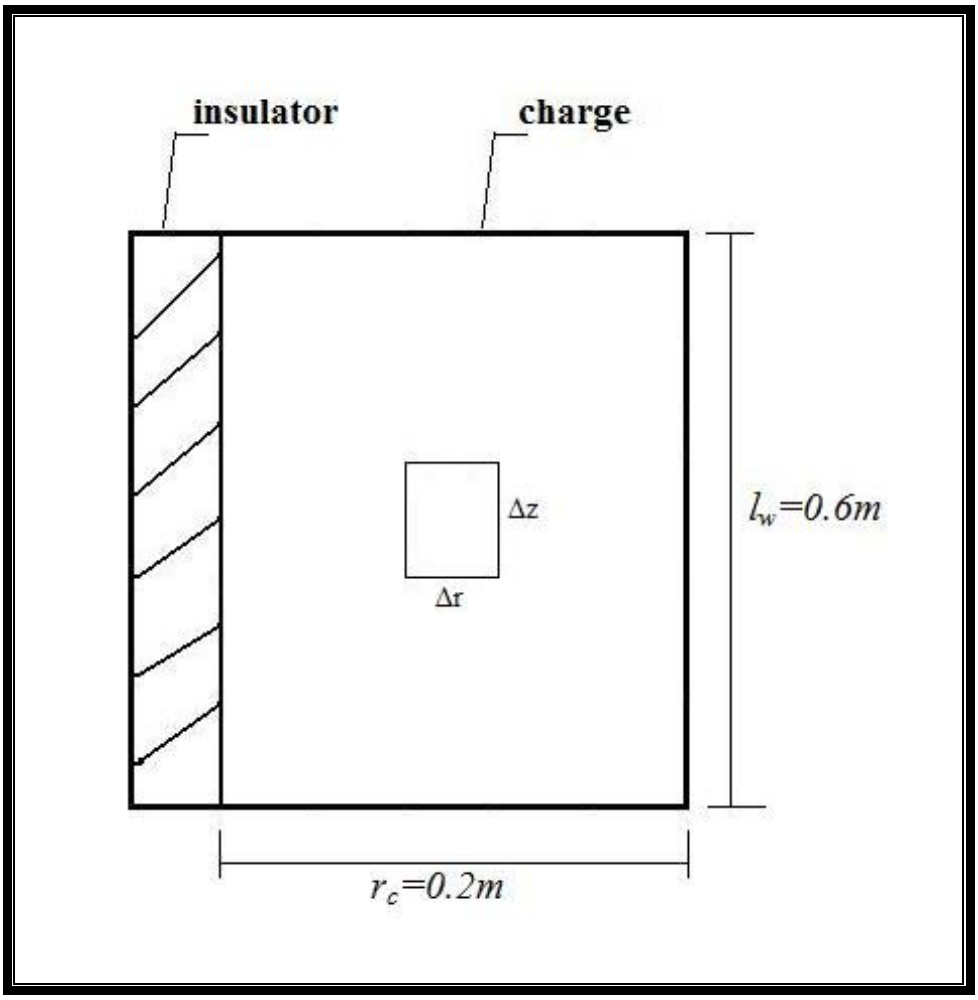

Figure (3.6):Geometrical parameters of the furnace

3.5.1 MODEL VALIDITY:

Increasing the number of nodes of the furnace charge have no effect on the accuracy of the results. Figure (3.7) shows the effect of increasing the number of nodes on the computed results. There is a good agreement (almost coincide) between the five nodes model and more than five model (ten nodes

model). This figure also justifies the assumption made in section (3.3) for the heat generation in a node.

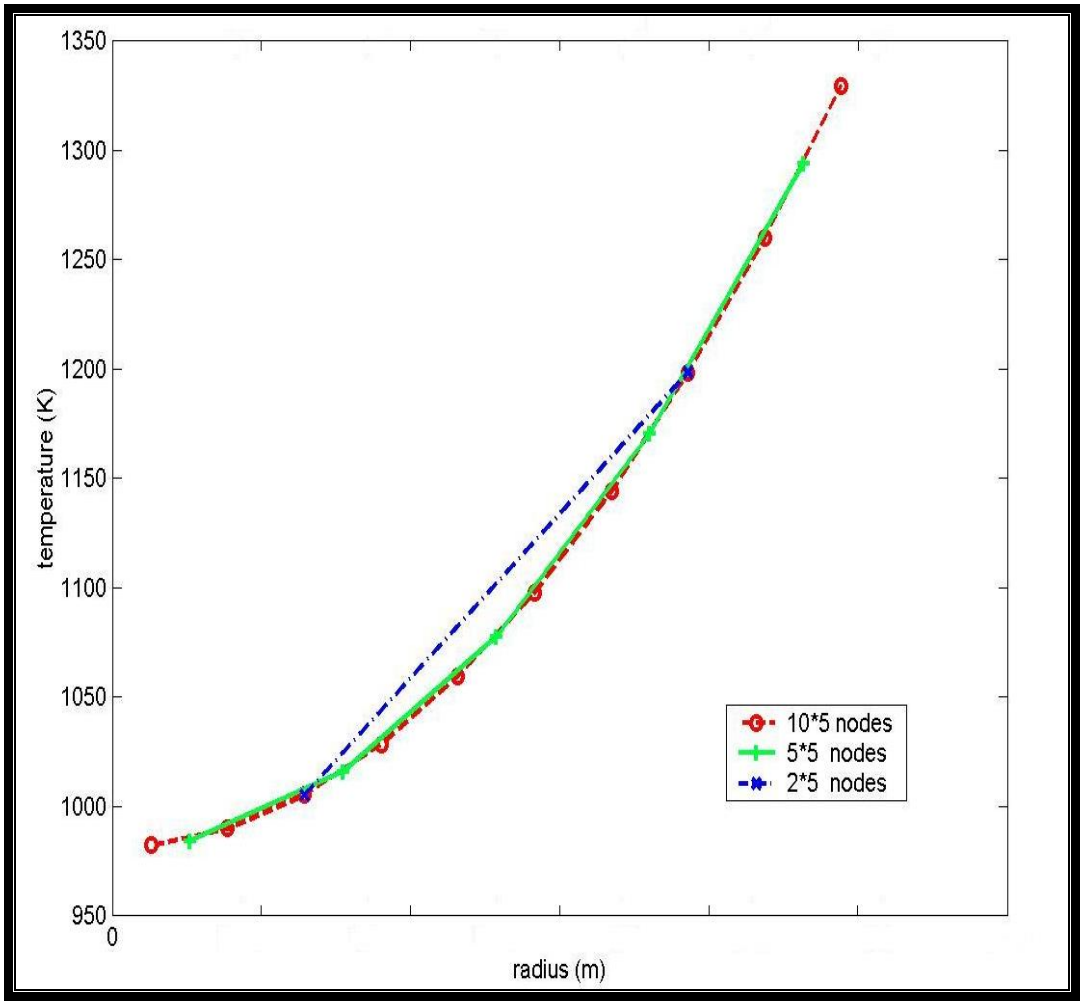

Figure (3.7): Number of nodes effect on the computational results

The mesh was constructed and programmed to simulate the furnace charge. The properties of the charge and the insulator and the power generation of each node were fed to the program. The limitation of this package is that the power generation must be calculated previously for each node and then entered as an input, and that the properties of the charge must be constant, except of course the magnetic permeability, where in iron its

change were taken into account because of its effect on the power generation as mentioned above.

3.5.2 CHARGE TEMPERATURE DISTRIBUTION:

Typical temperature-time curves for both iron and aluminum charges of the induction furnace described in chapter one, are shown in figures (3.8,9,10,11).

For iron charge the temperature at the surface, at the node (3,3), and at the node (1,3) are plotted against the heating time. The change of the slope of the curves is due to the effect of the Curie point and its effect on the permeability of the charge. Below this point the surface temperature is much higher than the temperature at the other nodes. As the temperature reaches the Curie point the permeability of the iron drops to unity and power generation is decreased as given by Eq. (3.10), accordingly the heating rate is decreased. The temperature rise curves of the nodes (3,3) and (1,3) are primarily due to the heat conducted from the surface of the charge rather than by the heat generation.

Naturally, if the heating is continued the charge temperature will also continue to rise even when the melting point is reached. In order to avoid this continuity and to simulate a proper melting process a simple ON-OFF controller is used. This controller depends on the lowest temperature of the nodes, which is obviously the node (1,3), so when the temperature of this

node reaches thirty degree above the melting temperature the controller will switch off the power source. The temperature rise curves of the iron charge are shown in figures (3.8) and (3.9).

Figures (3.10) and (3.11) illustrate the temperature-time curves for an aluminum charge which has a permeability of unity. So the power generation is constant during all the melting process and the effect of the Curie point is absent.

A limit switch has been used, just like in the iron charge, in order to provide an upper limit temperature for the molten aluminum. This controller also depends on the temperature of the node (1,3).

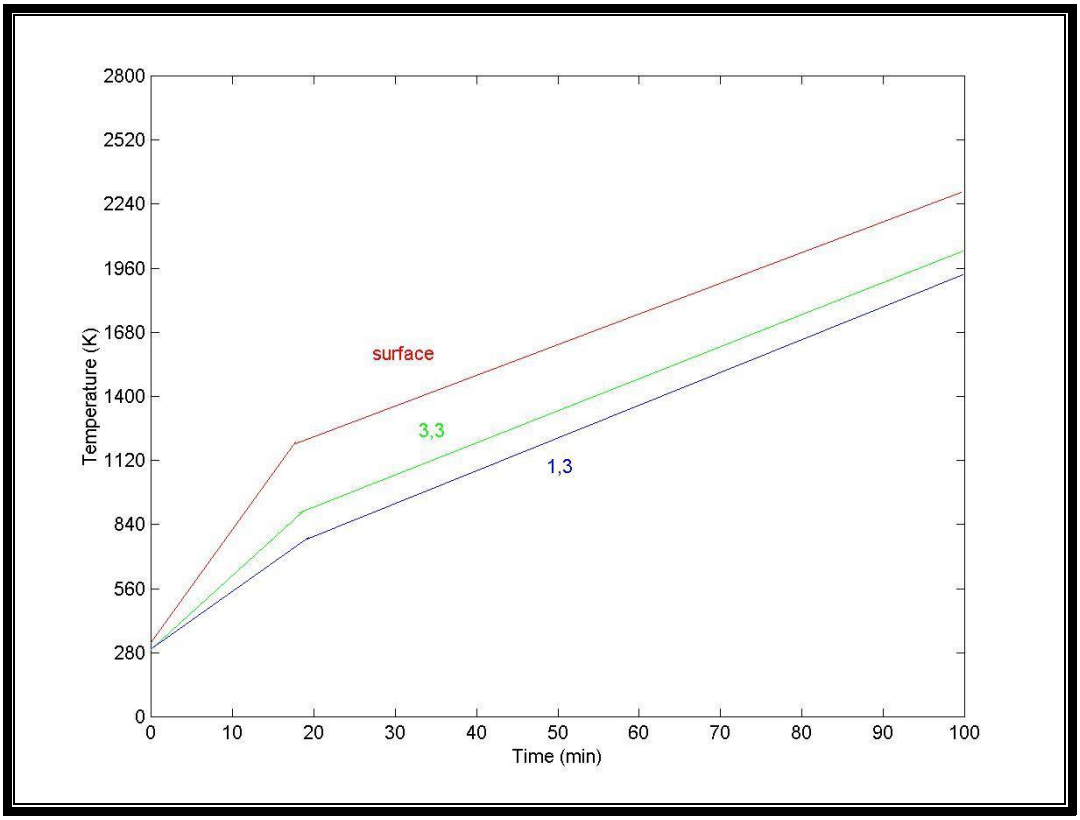

Figure (3.8): Temperature distribution for iron charge

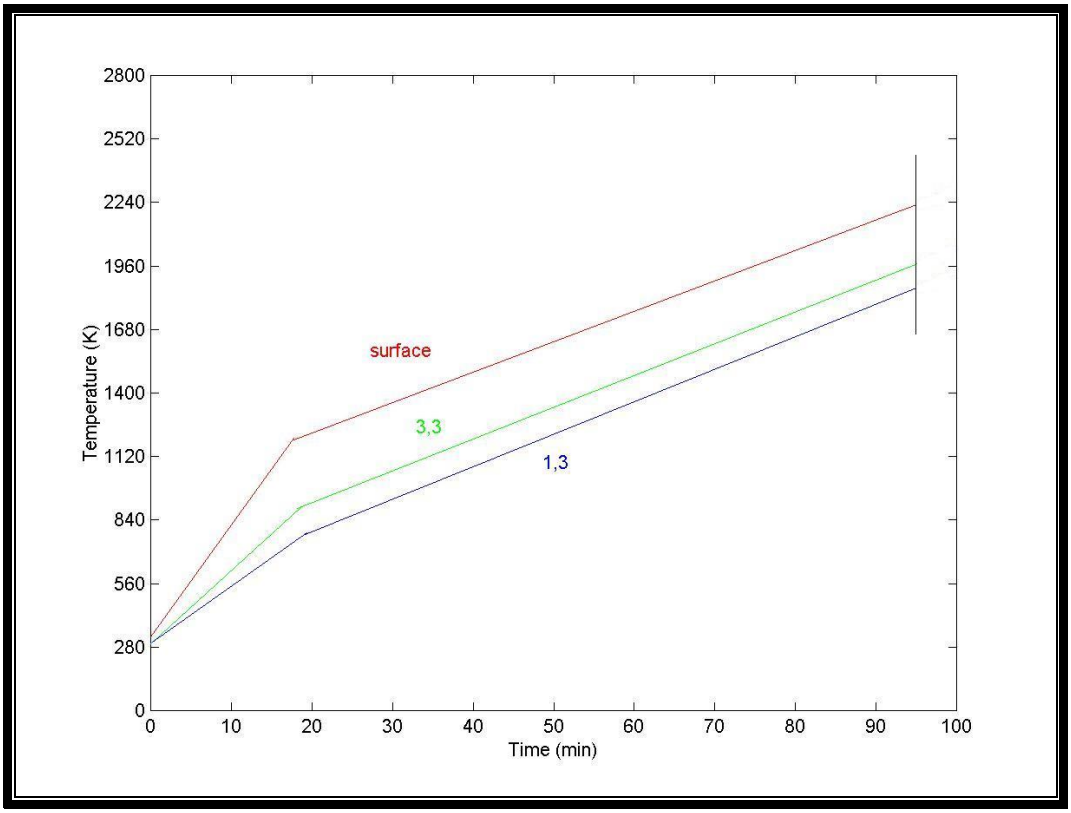

Figure (3.9): Temperature distribution with a limit switch for iron

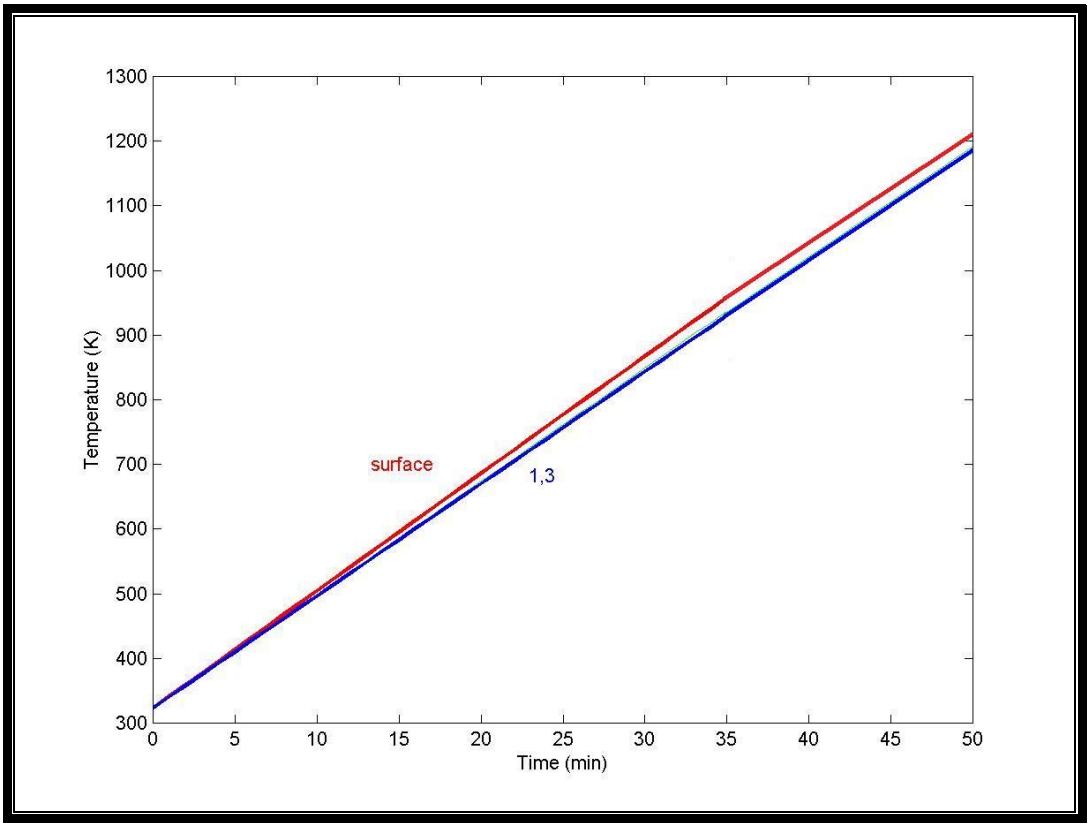

Figure (3.10): Temperature distribution for aluminum charge

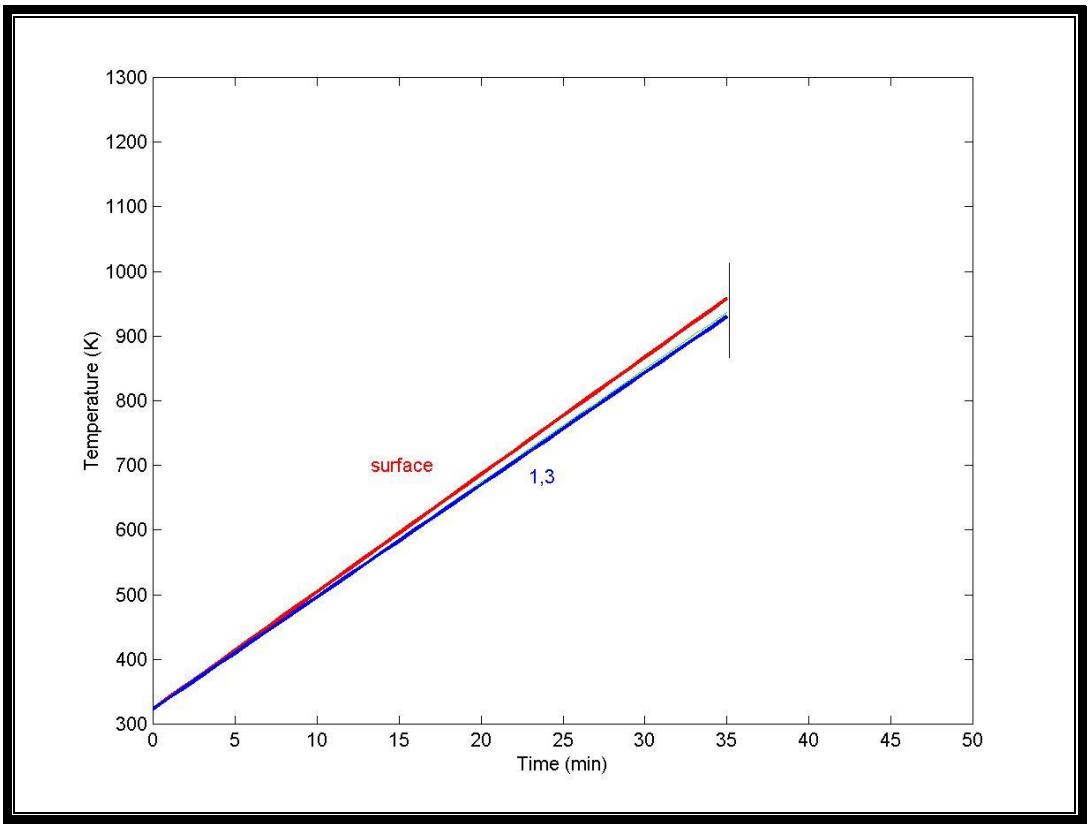

Figure (3.11): Temperature distribution with limit switch for aluminum

4.1 INTRODUCTION:

State estimation is the process of assigning a value to an unknown system state variable based on measurements from that system according to some criteria. Usually, the process involves imperfect measurements that are redundant and the process of estimating the system state is based on a statistical criterion that estimates the true value of the state variables [6]. A commonly used and familiar criterion is the weighted least squares approach (WLS) which is based on minimizing the sum of the squares of the differences between the estimated and " actual" (i.e. measured) values of functions. A very useful feature of a state estimation calculation is the ability to calculate (or estimate) quantities not being measured. This is most useful in cases of failure of communication lines connecting measuring devices to thermal processor or when these devices fails. A state estimator can “smooth out” small random errors in sensor readings, detect and identify gross measurement errors and “fill in” instrument readings that have failed due to communication failures, or any other malfunction.

State estimators may be either of a static or dynamic type. This chapter is concerned with the development of a static state estimator, capable of predicting (estimating) charge temperature of an induction furnace. The estimator is developed to produce the “best estimate" of the furnace temperatures and power supply recognizing that there are errors in the measured quantities and that there may be redundant measurements. The

output data can then be used in other thermal processor functions such as the control of the melting process[6].

4.2 MEASUREMENT SYSTEM MODEL:

The overall construction of the estimator is composed of three parts: the simulation of the furnace, the measurement system and the estimator itself. The construction of the estimator is illustrated by the flow chart given by figure (4.1). The furnace simulation represented by block 1 was developed in chapter three. Block 2 is a model of the measurement system developed here in sections (4.2.1-4.2.4) in which the raw measurements are generated by adding an appropriate noise to each measurement. In real life systems, however, these measurements are actual field instrument readings. The measurement system model is very important for the function of the estimator itself and for the case of instrument or communication lines failure.

The derivation of the measurement equations depends to a great extent on the locations of the sensors. The principal quantities measured are temperature, electric power and cooling water mass flow rate. Owing to the construction and operational conditions of the furnace, some quantities cannot be measured easily (mainly charge temperature). Each measurement in each part can be expressed in the form of an equation in terms of the state variables.

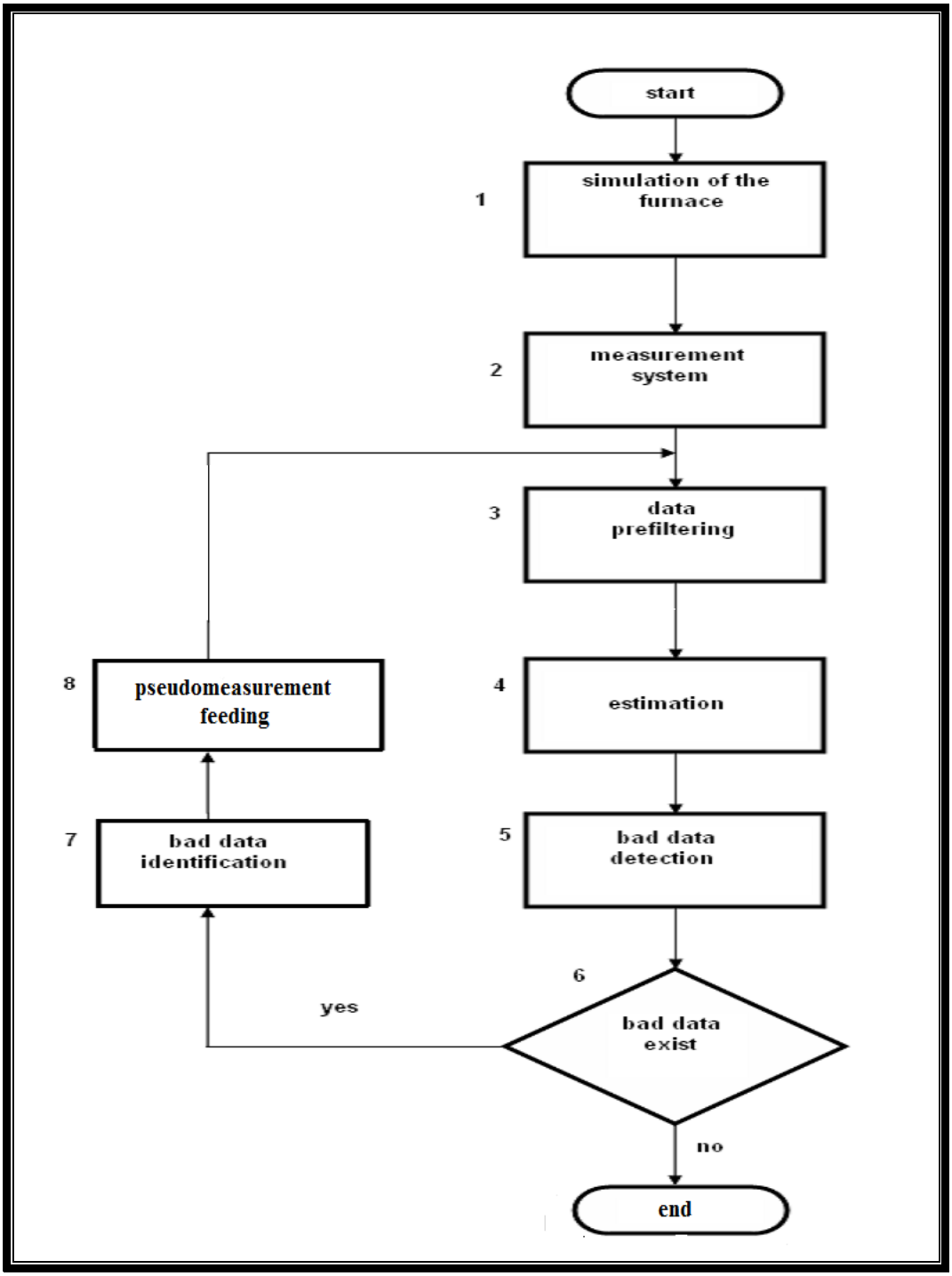

Figure (4.1): Flow chart of the estimator

Figure (4.2) shows a sketch for the proposed locations of the set of the measuring sensors adopted for the design of a static state estimator for an induction furnace. It is assumed that the following quantities are measurable : the temperature of the insulator at nodes s_1, s_2, s_3, and s_4 (T_1, T_2, T_3 and T_4),

the heat transferred from the charge towards the cooling water (Q_l), the temperatures of the water at the inlet and outlet of the cooling coil (T_{in} and T_{out}), the mass flow rate of the cooling water (M_w) and finally the electrical power(p_t) and the equivalent heat input at the terminals of the induction coil (p_{acl}).

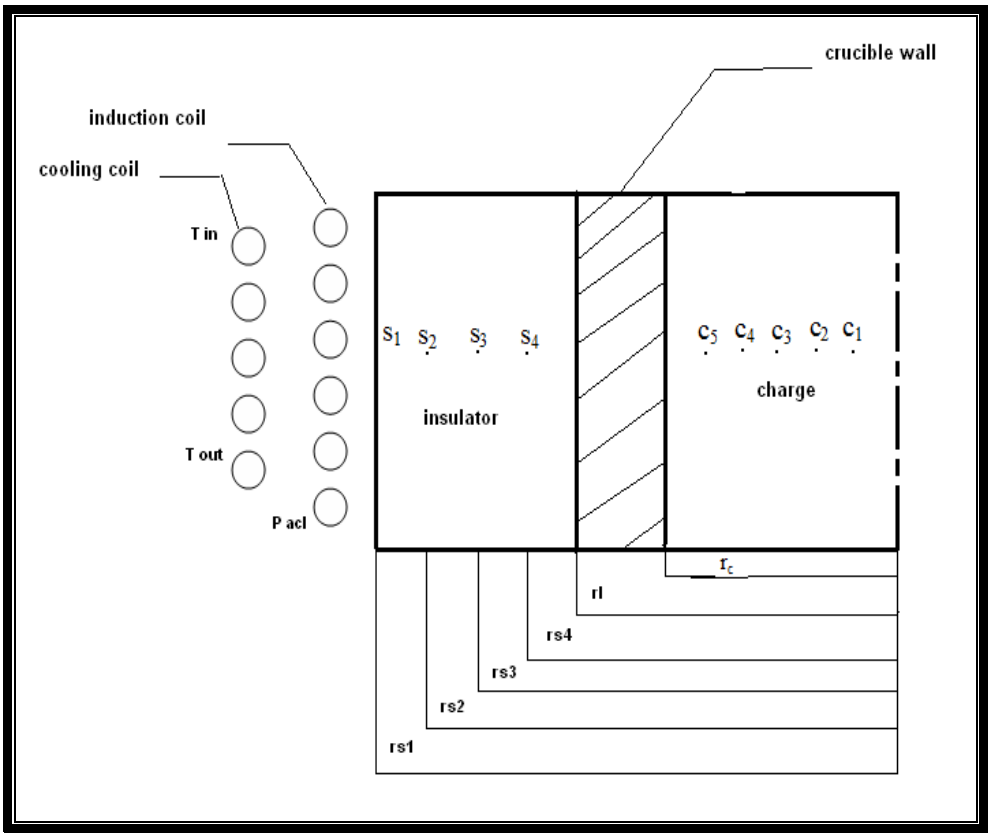

Figure (4.2): The proposed measuring system

In order to facilitate a mathematical formulation while still retaining the essential feature of the furnace, some assumptions have been made. General assumptions used for the whole system are given as follow:

1. The thermal properties of the charge, cooling water and the insulator are constant.

2. The kinetic and potential energies are neglected in the energy equations.
3. The mass flow rate of the cooling water is constant during the melting process.

To derive the governing measurement equations, the induction furnace is divided into three sections: crucible wall and the insulator, cooling coil and induction coil as detailed in the following sections.

4.2.1 CRUCIBLE WALL AND THE INSULATOR:

As shown in figure (4.2), four different positions inside the insulator are proposed (theoretically) to locate thermocouple junctions. These thermocouples provide an on-line temperature measurement to the estimator for the continuous prediction of the charge temperature.

In the steady state, the radial heat transfer equation can be applied in order to obtain the measurement equations which relates the temperatures at nodes s_1, s_2, s_3, and s_4 of figure (4.2) and the temperature at the surface of the charge T_c, which is given by:

$$T_c = (\text{heat generated} / Mc*C_p) + T_{initial} \quad \ldots (4.1)$$

The power used to melt the charge could be expressed by:

$$P_w = p_t - qhc \quad \ldots (4.2)$$

Where, *qhc* is the power lost in the induction coil which is given by [21]:

$$qhc = \frac{I_c^2 \cdot no^2 \rho_e \pi d_c^2}{\delta_c l_c} \quad \ldots (4.3)$$

The mass of the charge is given by:

$$M_c = \rho \pi r_c^2 l_w \quad \ldots (4.4)$$

Then, by substituting equations (4.2,3,4) in equation (4.1) the latter could be written as:

$$T_c = \frac{(p_t - qhc)t}{\rho \pi r_c^2 l_w C_p} + T_{initial} \quad \ldots (4.5)$$

Since the heat lost through the crucible wall and the insulator is constant, so the temperature at the node s_1 of the insulator is given by:

$$\frac{2\pi l_w (T_c - T_1)}{\frac{1}{k_z}\ln\frac{r_l}{r_c} + \frac{1}{k_{ins}}\ln\frac{r_{s1}}{r_l}} = \frac{2\pi l_w (T_c - T_{in})}{\frac{1}{k_z}\ln\frac{r_l}{r_c} + \frac{1}{k_{ins}}\ln\frac{r_{ins}}{r_l} + \frac{1}{k_{cu}}\ln\frac{r_w}{r_{ins}}} \quad \ldots (4.6)$$

Now let,

$haz = \frac{1}{k_z}\ln\frac{r_l}{r_c} + \frac{1}{k_{ins}}\ln\frac{r_{ins}}{r_l} + \frac{1}{k_{cu}}\ln\frac{r_w}{r_{ins}}$, and

$b = \frac{1}{k_z}\ln\frac{r_l}{r_c} + \frac{1}{k_{ins}}\ln\frac{r_{s1}}{r_l}$

Solving Eq. (4.6) for T_1 and simplifying with the above substitutions, one could obtain:

$$T_1 = T_c - \frac{T_c - T_{in}}{haz} * b \quad \ldots (4.7)$$

Similarly, the temperatures of the other nodes of the insulator which are s_2, s_3,and s_4 can be computed as:

$$T_2 = T_c - \frac{T_c - T_{in}}{haz} * b_1 \quad \ldots (4.8)$$

$$T_3 = T_c - \frac{T_c - T_{in}}{haz} * b_2 \quad \ldots (4.9)$$

$$T_4 = T_c - \frac{T_c - T_{in}}{haz} * b_3 \quad \ldots (4.10)$$

Where,

$$b_1 = \frac{1}{k_z} \ln \frac{r_l}{r_c} + \frac{1}{k_{ins}} \ln \frac{r_{s2}}{r_l} \quad ,$$

$$b_2 = \frac{1}{k_z} \ln \frac{r_l}{r_c} + \frac{1}{k_{ins}} \ln \frac{r_{s3}}{r_l} \quad \text{, and}$$

$$b_3 = \frac{1}{k_z} \ln \frac{r_l}{r_c} + \frac{1}{k_{ins}} \ln \frac{r_{s4}}{r_l}$$

The heat transferred from the charge towards the cooling coil through the crucible wall and the insulator can be expressed as:

$$Q_l = \frac{2\pi d_w (T_c - T_{in})}{haz} \quad \ldots (4.11)$$

4.2.2 COOLING COIL:

The temperature of the water at the outlet of the cooling coil can be expressed in terms of the mass flow rate of the cooling water (M_w), the temperature of the water at the inlet of the cooling coil (T_{in}), and the heat transferred from the charge towards the cooling coil through the crucible wall and the insulator (Q_l), as:

$$T_{out} = T_{in} + \frac{qhc + Q_l}{C_{pw}.M_w} \quad \ldots (4.12)$$

Where, *qhc* and Q_l are given by equations (4.3) and (4.11) respectively.

4.2.3 INDUCTION COIL:

The equivalent heat supplied at the terminals of the coil can be expressed in terms of the electrical power at the terminals of the coil as:

$$P_{acl} = p_t * t \quad \ldots (4.13)$$

Where, (p_t) is the electrical power supplied to the coil.

4.2.4 MEASUREMENT AND STATE VECTORS:

Arranging all the above defined measurements into a vector called "*Z*", one can get a system model in terms of the state variable vector "*X*", this can be represented in a general compact form as:

$Z = f(X)$ … (4.14)

Where, f(*X*) indicates the 10 measurement equations, i.e., Nm = 10.

$Z = [T_1, T_2, T_3, T_4, Q_l, p_t, P_{acl}, M_w, T_{in}, T_{out}]$ … (4.15)

The three elements of the state vector *X*, i.e., Ns = 3, are given by:

$X = [p_t, M_w, T_{in}]$ … (4.16)

Thus, the measurement redundancy is taken as the number of measurements divided by number of states which is equal to 3.33 which is a very good modification, where in the estimator developed by Al-Ubaidy [6] the redundancy was 2.

The temperature distribution inside the charge is immeasurable. It is necessary to establish five equations in order to predict the temperatures of the five nodes as mentioned in chapter 3. The equations can be found by considering steady-state radial heat transfer conditions from the surface of the charge, i.e., the outer radius, by using the equation of cylindrical heat transfer with heat generation at the surface [24], so the temperature at the node c_1 could be expressed as:

$$T_{c1} = Tc - \frac{P_6}{4 * k_c}(r_c^{\,2} - r_{c1}^2) \quad \text{… (4.17)}$$

Where, P_6 is the power generated at the surface of the charge per unit volume, which could be expressed as:

$$P_6 = \frac{P_w}{A_w l_w} \quad \ldots (4.18)$$

Similarly, the temperature of the other nodes of the charge which is c_2, c_3, c_4, and c_5 could be computed as:

$$T_{c2} = T_c - \frac{P_6}{4 * k_c}(r_c{}^2 - r_{c2}^2) \quad \ldots (4.19)$$

$$T_{c3} = T_c - \frac{P_6}{4 * k_c}(r_c{}^2 - r_{c3}^2) \quad \ldots (4.20)$$

$$T_{c4} = T_c - \frac{P_6}{4 * k_c}(r_c{}^2 - r_{c4}^2) \quad \ldots (4.21)$$

$$T_{c5} = T_c - \frac{P_6}{4 * k_c}(r_c{}^2 - r_{c5}^2) \quad \ldots (4.22)$$

4.3 THE ESTIMATOR:

The first part of the estimator is the data prefiltering, illustrated in block 3 of figure (4.1) in which data validation will be evaluated and substantiated. The data prefiltering usually consists of limit checking, simple

logic process prevents measurements read by failed transducers from entering the estimation process.

After the data prefiltering process, the measurements enter the estimation process, block 4 of figure (4.1), which is the main body of the estimator. This procedure can be built from various different algorithms. The WLS approach is a common and effective one and is adopted here because the WLS can display a good filtering performance without prior knowledge of the probability density function of the estimates which is required by other methods [11,25].

The WLS algorithm is designed on the assumption that the measurement noise has a Gaussian distribution. Generally speaking, an estimation algorithm cannot eliminate the BD influence in the estimation. When BD is present in the measurements, two cases are possible; first, the estimation algorithm may diverge. This problem can be avoided by the prefiltering process. Second, the estimation algorithm converges to a final solution after a number of iterations, but this result may be a long way from the true one. In this case, the detection-identification method is needed to eliminate BD from the measurements. This procedure is represented by blocks 5, 7, and 8 of figure (4.1).

The function of bad data detection is to find out whether BD exists in the measurements. A statistical test for BD detection is carried out

immediately after the estimation process. If BD is detected, identification is needed to detect the location of the BD in the measurement vector.

4.3.1 THE ESTIMATION ALGORITHM:

Based on the measurement equations developed in section 4.2. The measurements can be modeled as the combination of the actual measurements and the measurement noises, so the measurement process can be expressed as:

$$Z = f(X) + \theta \quad \ldots (4.23)$$

The elements of θ are Gaussian distribution random variables with zero mean and one standard deviation (σ). For the non-linear measurement system the WLS takes the following iterative form for the state estimates [26]:

$$\Delta X^* = [\,[H]^T[R]^{-1}[H]\,]^{-1}\,[H]^T\,[R]^{-1}\,[Z - f(X)] \quad \ldots (4.24)$$

Where [R] is the weighted matrix, it is $(\sigma_1^2, \sigma_2^2, \ldots\ldots, \sigma_m^2)$ diagonal matrix, and the elements give an indication of the accuracy of the corresponding measurements, so the *i*'th element of [R] is taken as [26]:

$$r_{ii}^{-1} = \frac{1}{\sigma_i^2} \quad \ldots (4.25)$$

And [H] is the Jacobian matrix and is given by:

$$[H] = \frac{\partial f(X)}{\partial X} \quad \ldots (4.26)$$

The elements of the Jacobian matrix H of the measurement equations could be determined by differentiating Eqs. (4.7) to (4.13) by using their appropriate substitutions, for example by differentiation of Eq.(4.7) we obtain:

$$H(1,1) = \frac{\partial T_1}{\partial p_t} = (1 - \frac{b}{haz}) \frac{t}{\rho \pi r_c^2 l_w C_p} \quad ,$$

$$H(1,2) = \frac{\partial T_1}{\partial T_{in}} = \frac{b}{haz} \quad , \text{ and}$$

$$H(1,3) = \frac{\partial T_1}{\partial M_w} = 0$$

Similarly, the other elements could be expressed as:

$$H(2,1) = (1 - \frac{b_1}{haz}) \frac{t}{\rho \pi r_c^2 l_w C_p} \quad ,$$

$$H(2,2) = \frac{b_1}{haz} \quad ,$$

$$H(3,1) = (1 - \frac{b_2}{haz}) \frac{t}{\rho \pi r_c^2 l_w C_p} \quad ,$$

$$H(3,2) = \frac{b_2}{haz} \quad ,$$

$$H(4,1) = (1 - \frac{b_3}{haz}) \frac{t}{\rho \pi r_c^2 l_w C_p} \quad ,$$

$$H(4,2) = \frac{b_3}{haz} \quad ,$$

$$H(5,1) = \frac{2}{haz} \frac{t}{\rho r_c^2 C_p} \quad ,$$

$$H(5,2) = -\frac{2\pi l_w}{haz} \quad ,$$

$$H(6,1) = 1 \quad ,$$

$$H(7,1) = t \quad ,$$

$$H(8,2) = 1 \quad ,$$

$$H(9,3) = 1 \quad ,$$

$$H(10,1) = \frac{2}{haz \cdot C_{pw} \cdot M_w} \frac{t}{\rho r_c^2 l_w} \quad ,$$

$$H(10,2) = 1 - \frac{2\pi l_w}{haz \cdot C_{pw} \cdot M_w} \quad , \text{ and}$$

$$H(10,3) = -\frac{qhc + Q_l}{C_{pw} \cdot M_w^2}$$

The remaining elements of the Jacobian matrix are zero

The iterations continue until a tolerance $\left|x_i^{k+1} - x_i^k\right| < \varepsilon$ is satisfied where the superscript k denotes the iteration cycle, ε represents accuracy bounds and it is set equal to 10^{-5}.

The initial values of the elements of the state variables X^0 are taken arbitrarily around the nominal working point. Figure (4.3) shows the state estimation solution algorithm, which is represented by block 4 of figure (4.1).

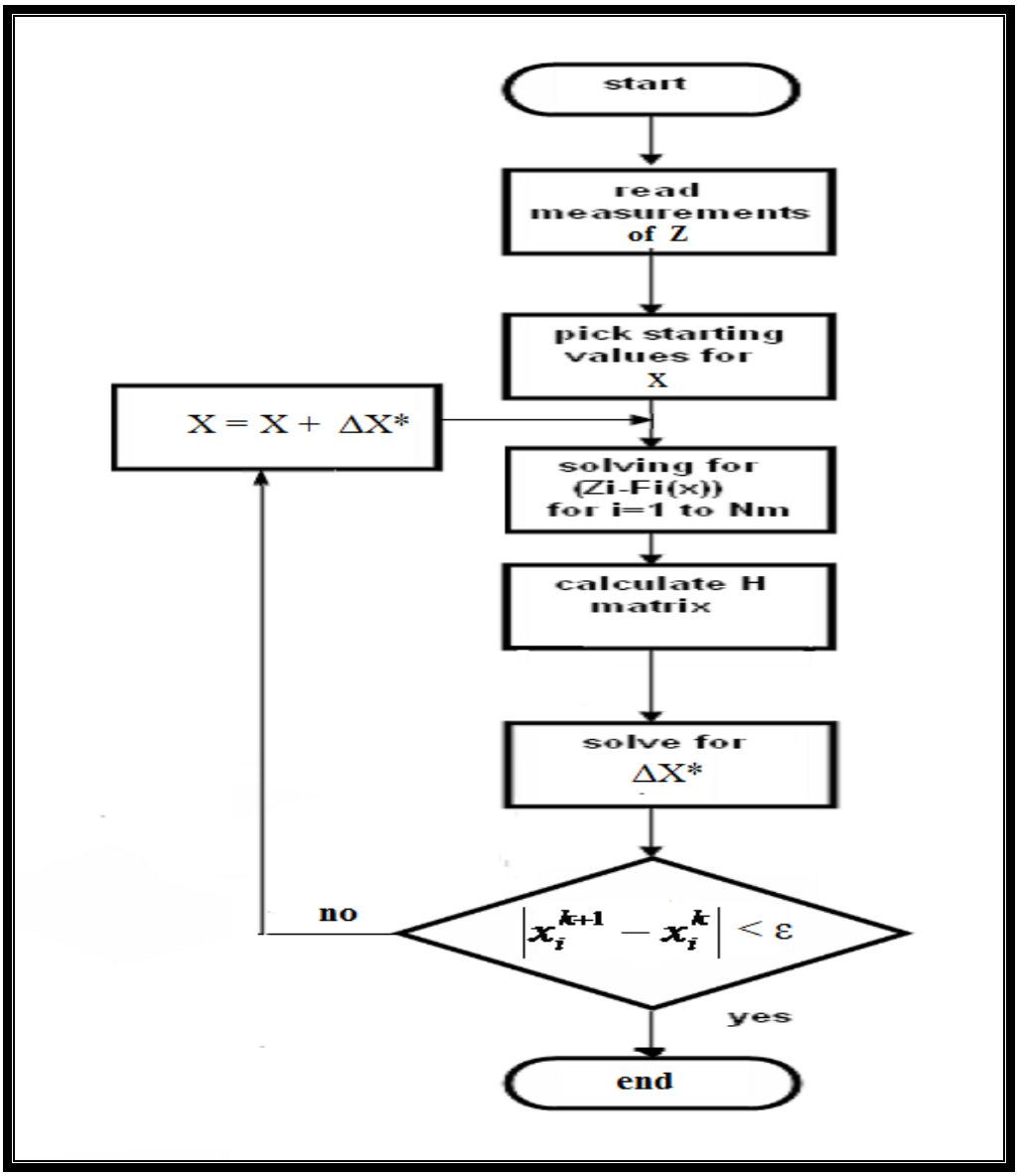

Figure (4.3): State estimation solution algorithm

4.3.2 DETECTION OF BAD DATA:

Bad data detection, block 5 of figure (4.1), is carried out by using a statistical criterion known as sum of the squared residuals or J-index test [16]. It is based on the residual of the measurements of vector Z and standard deviation of each of these measurements. The measurement residual (r_j) is the deviation between the measurements and the estimates and can be written as:

$$r_j = Z - f(X) \quad \ldots (4.27)$$

The value of the J-index is the statistical variable which is defined as the sum of the weighted squares of all the measurement residuals [16]. This definition is expressed as:

$$J(x) = \sum_{i=1}^{Nm} \frac{r_j^2(i)}{\sigma_i^2} \quad \ldots (4.28)$$

In the normal case when there are no BD, measurements only suffer from a Gaussian distribution of random noise indicated by the vector θ in Eq. (4.23), and the measurement residual r_j exhibits a normal distribution. J(x) is a chi-square distribution with a degree of freedom of the measurements equal to the difference between number of measurements and number of states, i.e., Nm-Ns; for the present work it is 10 - 3 =7. The detection threshold value t_j can be determined from the chi-square distribution tables after the significance level (α) is specified. If J(x) is smaller than t_j, then the resultant estimate is treated as free of BD. However, when the value of J(x) is higher

than the threshold, it is assumed that there is some BD in the measurements. The process of BD identification is then started.

In the present work, the value of α was specified as 0.025 hence for a seven degree of freedom the value of the detection threshold t_j becomes 16.01 [27].

4.3.3 BAD DATA IDENTIFICATION:

In order to appoint the location of the bad data, consider the measurement of temperature of a particular part. Call this measured value z_i, which has a corresponding pseudo measurement z_{pi}. Figure. (4.4) shows a plot of the normal probability density function of z_i (or z_{pi}), since the error in z_i (or z_{pi}) is assumed normally distributed with zero mean value, the probability density function is centered on the true value of z_i. Since the error on all the measurements are assumed normal, the estimate, X*, are assumed approximately normally distributed and that any quantity that is a function of X is also approximately normally distributed quantity. In figure (4.5) the probability density function for the calculated temperature f_i, which is a function of the estimated state, X*, is shown. The difference between the estimate, f_i, and the measurement, z_i, is called the measurement residual and is designated y_i. The probability density function for y_i is also normal and is shown in figure (4.6) as having zero mean and a standard deviation (σ_{yi}). If

the measurement residual is divided by (σ_{yi}), a normalized measurement residual is obtained. It is designated y_i^{norm} and is shown in figure (4.7) along with its probability density function, which is normal and has a standard deviation of unity [6].

The computational procedure is to calculate the normalized measurement residuals y_i^{norm} for each measurement. Measurements having the larger absolute normalized residual are labeled as prime suspects. These prime suspects are removed from the estimator and can be replaced by their corresponding pseudo measurements [16]. This procedure is implemented by block 7 of figure (4.1), which can be expressed mathematically as;

$$y_i^{norm} = \frac{z_i - f_i(x^*)}{\sigma_{yi}} \quad \ldots (4.29)$$

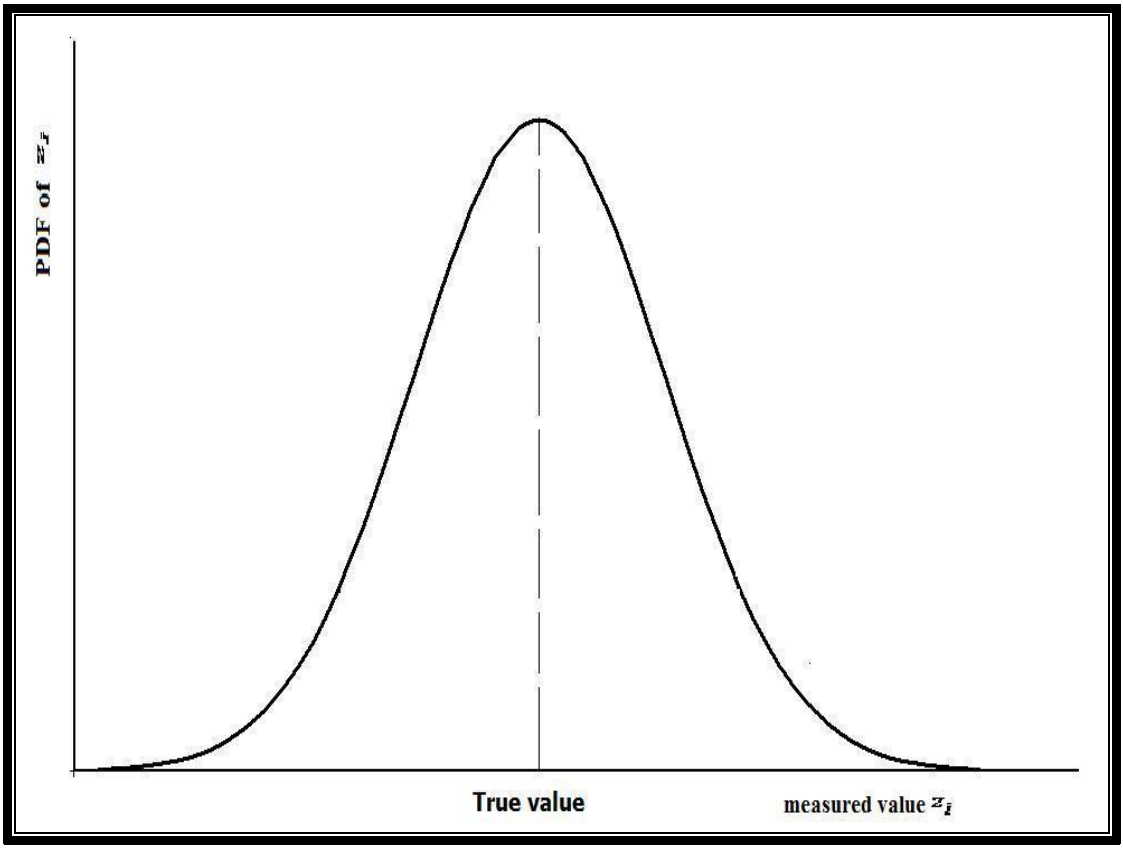

Figure (4.4): Normal probability density function of z_i

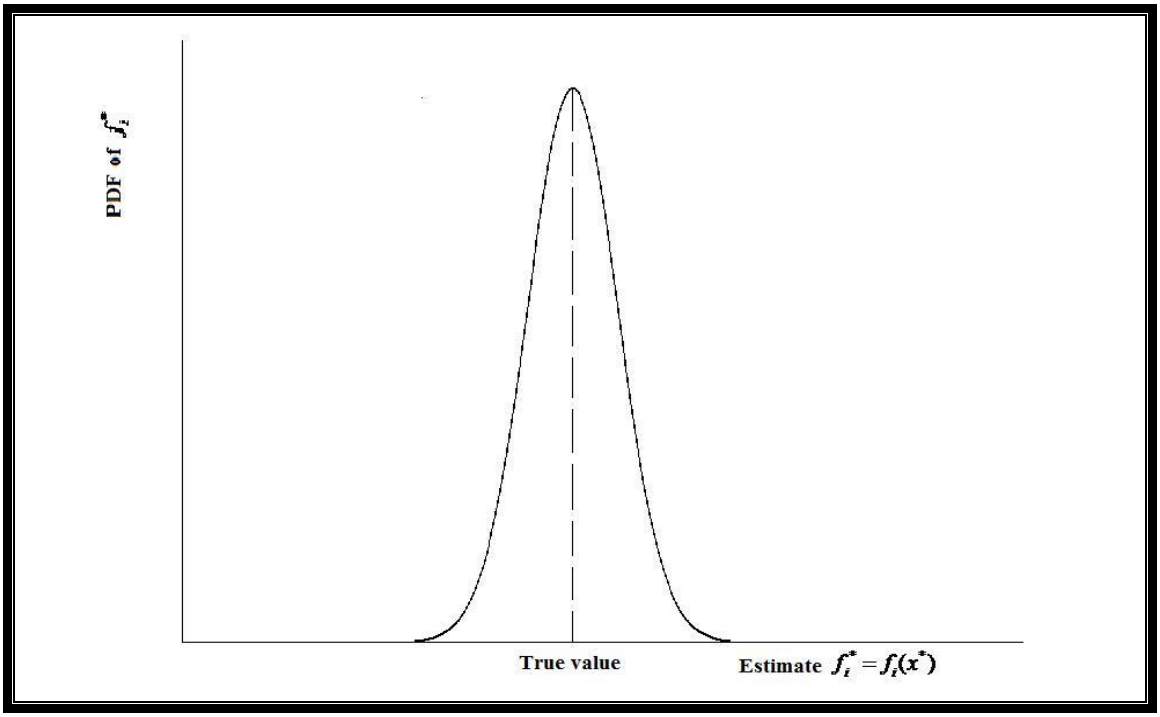

Figure (4.5): Probability density function of f_i^*

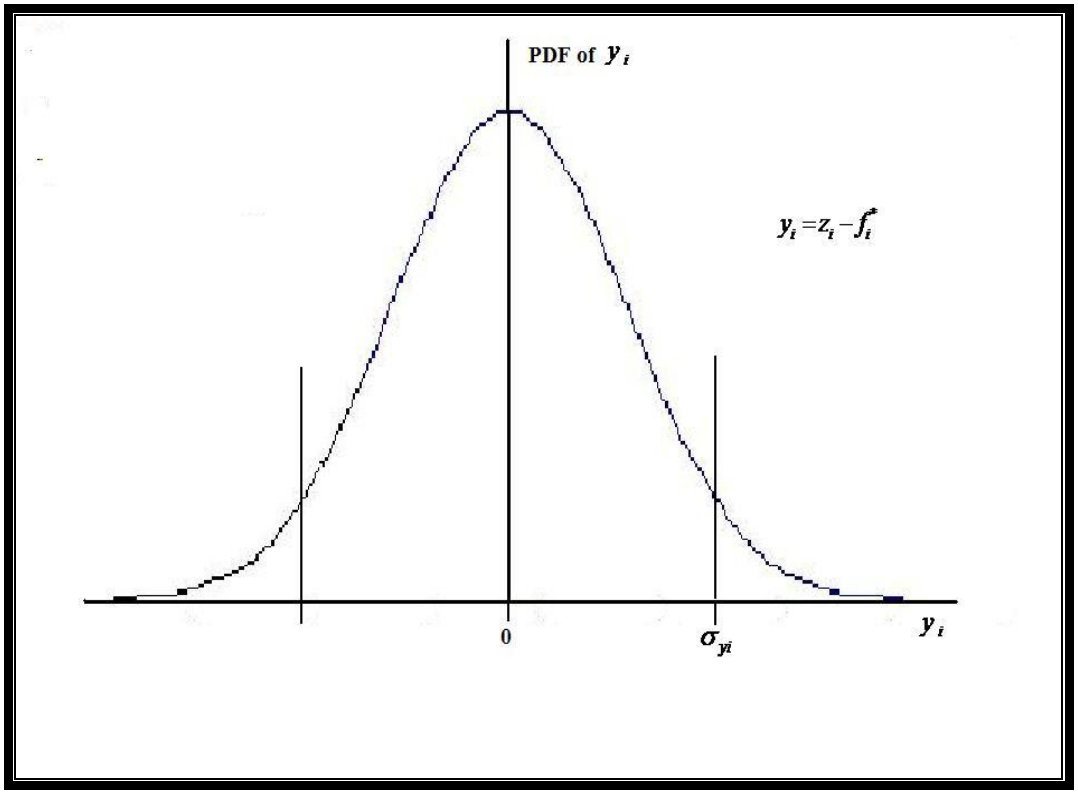

Figure (4.6): Probability density function of y_i

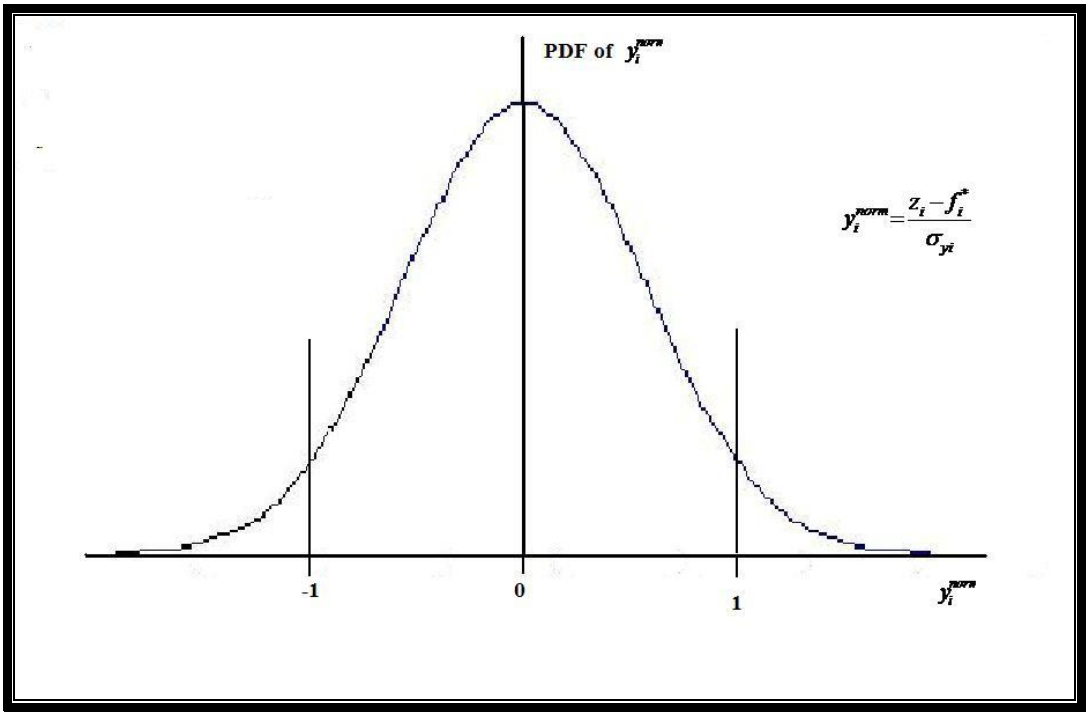

Figure (4.7): Probability density function of y_i^{norm}

4.4 TESTING INDICES:

The estimated results can be compared by a statistical test. In order to assess the performance of the estimator, two statistical indices S_e and S_m are used as defined below [25]:

$$S_e = \left[\frac{1}{Nm} \sum_{i=1}^{Nm} \left(\frac{z_{ei} - z_{ti}}{\sigma_i} \right)^2 \right]^{1/2} \quad \text{... (4.30)}$$

$$S_m = \left[\frac{1}{Nm} \sum_{i=1}^{Nm} \left(\frac{z_{mi} - z_{ti}}{\sigma_i} \right)^2 \right]^{1/2} \quad \text{... (4.31)}$$

Where S_e is the sum of the squares of the normalized deviation between the estimates and the true values of each variable of vector *Z*, while S_m is the sum of the squares of the normalized deviation between the measurements and the true values of each variable of vector *Z*. When S_e is smaller than S_m it shows that the estimator is effective in the filtering process. Generally speaking, the smaller S_e, the better the estimator in the filtering process.

4.4.1 MONITORING THE CHARGE TEMPERATURE:

A number of computer runs are made in order to test the estimator ability in filtering out the undesirable measurement Gaussian noise. Each test consist of a comparison between the true and the estimated values for all the variables in the measurement vector Z, Eq. (4.15). The true values of the variables of vector Z are determined from the measurement equations of

section 4.2 and the state vector X, Eq. (4.16). Vector X is taken from the furnace design analysis of chapter one. The measured values are then computed by using Eq. (4.23) where θ is a 10 dimensional noise vector and one standard deviation.

For the furnace charge node temperatures, the true values are determined approximately by the furnace dynamic thermal model of chapter three. While the estimated values are determined by using equations (4.17, 19, 20, 21, 22) which are based on the steady state conditions.

Tables (4.1,2,3,4) show a typical test results for the estimator for both aluminum and iron charge furnace. The first column list the ten measurement variables in the same order as defined by Eq. (4.15), while the last five variables are the charge node temperatures as defined by figure (4.1) for which there are no measurements. The tables also show the true, the measured, and the estimated values for each variable. Also they show the difference between the measured values and the true values, and the difference between the estimated values and the true values. The values of S_e, S_m, S_e/S_m, and J(x) are shown also for each table.

Table (4.1) shows the test results for an aluminum charge after melting, suffers only from the Gaussian noise. It showed that the estimator has predicts the charge node temperatures with less than 0.7% error. And the values of S_e, S_m, S_e/S_m, and J(x) are equal to 0.58638, 0.78242, 0.74944, and

0.8463 respectively, which indicates that the estimator works efficiently in filtering out the Gaussian noise.

Table (4.2) shows the least expected case in which all the ten measurements have an error of one standard deviation of 5% of the true value. The estimator still works efficiently where S_e/S_m is 0.6856 and the maximum node error is less than 2% .

Table (4.3) shows the estimated results for an iron charge also after the melting happens, and the measurements are suffer from just the Gaussian noise. The table showed that the error of the charge node temperatures is less than 1%, and the values of S_e, S_m, S_e/S_m, and J(x) are equal to 0.63248, 0.78351, 0.80723, and 1.09267 respectively.

In table (4.4), all the measurements have an error of one standard deviation of 5% of the true value. Again the estimator works efficiently in filtering out the Gaussian noise and estimating the charge node temperatures, where the maximum error of the node temperatures is about 2%.

A comparison between the tables of the aluminum charge and those of the iron charge shows that the estimator works more efficiently for the aluminum charge which is nonmagnetic material than for the ferrous materials, mainly because of the Curie point effect where the heating rate have changed.

4.4.2 ESTIMATOR PERFORMANCE WITH BAD DATA:

Errors may be introduced into the measurements mainly because of the calibration bias in the sensor, the corruption in the communication lines, and inaccuracy of the analog to digital converter. Under normal operating conditions, the magnitudes of the error caused by the noise sources are small, the developed estimator is found to work efficiently under such conditions, as discussed above. But in an induction melting furnace, the working environment is very hard and the operating conditions are not normal. So the probability of the failure of the measurement equipments or at least its malfunction is very probable, errors happened because of this condition are called the bad data (BD) and the estimator should be able to work with such errors.

The estimator was run with the feeding of a single bad data measurement of size 5σ where σ is taken five percent of the true value .

The variable selected for this test is the temperature of the insulator node number 3, i.e., T_{s3}. The presence of bad data did not prevent the estimator from convergence, table (4.5) presents the result of the estimator for the iron charge. The residual J(x) has increased to 20.6491 which is greater than the detection threshold t_j which is equal to 16.01 for a seven degree of freedom as mentioned above, this indicates the existence of a bad data.

The next step is to identify the bad data, which is successfully detected as measurement number 3. Identification was accomplished by using the

criterion given by Eq. (4.29). Even with the presence of bad data the estimator works efficiently in estimating the charge node temperatures with an error less than 2.2%.

In the iron charge the temperature at the surface exceeds 2200 Kelvin so the part of the insulator close to the charge suffer from a high temperatures, so the thermocouples at the nodes which close to the charge may damaged because of melting. So the test for assessing the ability of the estimator in handling the bad data will take into account this situation.

The estimator was run with feeding of two bad data which are the temperatures at nodes s_3 and s_4, i.e. T_{s3} and T_{s4} are equal to zero. Data prefiltering will detect this and a pseudo measurement is fed. Tables (4.6) and (4.7) investigates the possibilities of the pseudo measurements.

In table (4.6) the pseudo measurement is generated from the data files of the prior instant. While in table (4.7) these pseudo measurements are taken by replacing T_{s3} and T_{s4} with T_{s2}.

Another test for the performance of the estimator with the presence of bad data is made by using a very extreme condition which is a feeding of three bad data in the measurement i.e., about one third of the measurements are failing (bad data).

The three measurements taken as a bad data are the measurements of the thermocouples that located at the nodes s_2, s_3, and s_4 of the insulation.

The temperatures of those three nodes i.e., T_{s2}, T_{s3}, and T_{s4} are taken equal to zero, and the pseudo measurement of each one of them are taken by replacing it with the measurement of the thermocouple that located at node s_1 of the insulator i.e., T_{s1}, so the insulator is assumed to be in the same temperature at all the nodes.

The presence of three bad data did not prevent the estimator from convergence, and it is still works efficiently even at this condition, this is be clear from the values of S_e, S_m, and S_e/S_m which are equal to 1.76352, 2.6683, and 0.66091 respectively. The results of this test are listed in table (4.8).

TABLE (4.1): ALUMINUM CHARGE WITH GAUSSIAN NOISE

$S_e = 0.58638$

$S_m = 0.78242$

$S_e/S_m = 0.74944$

$J(x) = 0.8463$

Variable	True Value Z_t	Measured Value Z_m	Estimated Value Z_e	Z_m-Z_t	Z_e-Z_t	Error %
T_{s1} (K)	$2.99*10^2$	$3.080*10^2$	$3.034*10^2$	9.00	4.4	
T_{s2} (K)	$4.638*10^2$	$4.661*10^2$	$4.660*10^2$	2.27	2.25	
T_{s3} (K)	$6.355*10^2$	$6.429*10^2$	$6.408*10^2$	7.413	5.32	
T_{s4} (K)	$8.144*10^2$	$8.395*10^2$	$8.268*10^2$	25.08	12.41	
Q_l (W)	$1.854*10^3$	$1.800*10^3$	$1.819*10^3$	-53.77	-34.72	
P_t (W)	$1.41*10^5$	$1.352*10^5$	$1.376*10^5$	$-5.67*10^3$	$-3.40*10^3$	
P_{acl} (J)	$2.961*10^8$	$2.92*10^8$	$2.894*10^8$	$-5.92*10^6$	$-6.23*10^6$	
M_w (kg/s)	2.3	2.3879	2.354	0.0879	0.054	
T_{in} (K)	$2.98*10^2$	$3.117*10^2$	$3.098*10^2$	13.74	11.8	
T_{out} (K)	$2.982*10^2$	$3.124*10^2$	$3.104*10^2$	14.23	12.2	
T_{c1} (K)	$9.531*10^2$	—	$9.466*10^2$	—	-6.516	0.68
T_{c2} (K)	$9.607*10^2$	—	$9.539*10^2$	—	-6.725	0.69
T_{c3} (K)	$9.735*10^2$	—	$9.673*10^2$	—	-6.118	0.62
T_{c4} (K)	$9.913*10^2$	—	$9.853*10^2$	—	-5.971	0.60
T_{c5} (K)	$1.014*10^3$	—	$1.008*10^3$	—	-5.366	0.53

$$error\,\% = \frac{|Z_e - Z_t|}{Z_t} * 100$$

TABLE (4.2): ALUMINUM CHARGE WITH ERROR OF ONE STANDARD DEVIATION FOR ALL THE MEASUREMENTS

$S_e = 0.6856$

$S_m = 1$

$S_e/S_m = 0.6856$

$J(x) = 0.92025$

Variable	True Value Z_t	Measured Value Z_m	Estimated Value Z_e	Z_m-Z_t	Z_e-Z_t	Error %
T_{s1} (K)	$2.99*10^2$	$3.139*10^2$	$3.112*10^2$	14.95	12.27	
T_{s2} (K)	$4.638*10^2$	$4.870*10^2$	$4.803*10^2$	23.19	16.49	
T_{s3} (K)	$6.355*10^2$	$6.672*10^2$	$6.597*10^2$	31.77	24.23	
T_{s4} (K)	$8.144*10^2$	$8.551*10^2$	$8.476*10^2$	40.72	33.13	
Q_l (W)	$1.854*10^3$	$1.761*10^3$	$1.792*10^3$	-92.71	-61.64	
P_t (W)	$1.41*10^5$	$1.339*10^5$	$1.364*10^5$	$-7.05*10^3$	$4.60*10^3$	
P_{acl} (J)	$2.961*10^8$	$2.812*10^8$	$2.876*10^8$	$-1.48*10^7$	$-8.4*10^6$	
M_w (kg/s)	2.3	2.415	2.361	0.115	0.061	
T_{in} (K)	$2.98*10^2$	$3.129*10^2$	$3.103*10^2$	14.9	12.3	
T_{out} (K)	$2.982*10^2$	$3.131*10^2$	$3.108*10^2$	14.91	12.6	
T_{c1} (K)	$9.531*10^2$	__	$9.374*10^2$	__	-15.76	1.65
T_{c2} (K)	$9.607*10^2$	__	$9.426*10^2$	__	-18.13	1.88
T_{c3} (K)	$9.735*10^2$	__	$9.582*10^2$	__	-15.25	1.56
T_{c4} (K)	$9.913*10^2$	__	$9.796*10^2$	__	-11.75	1.18
T_{c5} (K)	$1.014*10^3$	__	$1.004*10^3$	__	-9.698	0.95

TABLE (4.3): IRON CHARGE WITH GAUSSIAN NOISE

$S_e = 0.63248$

$S_m = 0.78351$

$S_e/S_m = 0.80723$

$J(x) = 1.09267$

Variable	True Value Z_t	Measured Value Z_m	Estimated Value Z_e	Z_m-Z_t	Z_e-Z_t	Error %
T_{s1} (K)	$3.89*10^2$	$4.006*10^2$	$3.992*10^2$	11.67	10.32	
T_{s2} (K)	$6.825*10^2$	$7.087*10^2$	$6.999*10^2$	26.22	17.43	
T_{s3} (K)	$1.080*10^3$	$1.116*10^3$	$1.102*10^3$	36.73	22.6	
T_{s4} (K)	$1.493*10^3$	$1.540*10^3$	$1.526*10^3$	47.18	32.93	
Q_l (W)	$4.729*10^3$	$4.604*10^3$	$4.637*10^3$	-124.28	-91.47	
P_t (W)	$1.41*10^5$	$1.367*10^5$	$1.388*10^5$	$-4.23*10^3$	$-2.11*10^3$	
P_{acl} (J)	$8.03*10^8$	$7.84*10^8$	$8.01*10^8$	$-1.9*10^7$	$-2.1*10^6$	
M_w (kg/s)	2.3	2.402	2.36	0.102	.06	
T_{in} (K)	$2.98*10^2$	$3.127*10^2$	$3.120*10^2$	14.7	14.01	
T_{out} (K)	$2.985*10^2$	$3.133*10^2$	$3.128*10^2$	14.81	14.3	
T_{c1} (K)	$1.842*10^3$	__	$1.825*10^3$	__	-17.12	0.92
T_{c2} (K)	$1.864*10^3$	__	$1.846*10^3$	__	-17.28	0.92
T_{c3} (K)	$1.899*10^3$	__	$1.882*10^3$	__	-16.81	0.88
T_{c4} (K)	$1.949*10^3$	__	$1.933*10^3$	__	-15.95	0.81
T_{c5} (K)	$2.013*10^3$	__	$1.997*10^3$	__	-15.61	0.77

TABLE (4.4): IRONCHARGE WITH ERROR OF ONE STANDARD DEVIATION FOR ALL THE MEASUREMENTS

$S_e = 0.76541$

$S_m = 1$

$S_e/S_m = 0.76541$

$J(x) = 1.1836$

Variable	True Value Z_t	Measured Value Z_m	Estimated Value Z_e	Z_m-Z_t	Z_e-Z_t	Error %
T_{s1} (K)	$3.89*10^2$	$4.084*10^2$	$4.066*10^2$	19.45	17.61	
T_{s2} (K)	$6.825*10^2$	$7.166*10^2$	$7.092*10^2$	34.12	26.7	
T_{s3} (K)	$1.080*10^3$	$1.134*10^3$	$1.117*10^3$	54.51	37.51	
T_{s4} (K)	$1.493*10^3$	$1.567*10^3$	$1.546*10^3$	74.66	53.42	
Q_l (W)	$4.729*10^3$	$4.492*10^3$	$4.577*10^3$	-236.45	-151.61	
P_t (W)	$1.41*10^5$	$1.339*10^5$	$1.357*10^5$	$-7.05*10^3$	$-5.27*10^3$	
P_{acl} (J)	$8.03*10^8$	$7.628*10^8$	$7.94*10^8$	$-4.09*10^7$	$-9.4*10^6$	
M_w (kg/s)	2.3	2.415	2.37	0.115	0.07	
T_{in} (K)	$2.98*10^2$	$3.129*10^2$	$3.122*10^2$	14.9	14.2	
T_{out} (K)	$2.985*10^2$	$3.134*10^2$	$3.131*10^2$	14.92	14.56	
T_{c1} (K)	$1.842*10^3$	__	$1.808*10^3$	__	-34.04	1.84
T_{c2} (K)	$1.864*10^3$	__	$1.825*10^3$	__	-39.14	2.09
T_{c3} (K)	$1.899*10^3$	__	$1.866*10^3$	__	-33.43	1.76
T_{c4} (K)	$1.949*10^3$	__	$1.920*10^3$	__	-29.23	1.49
T_{c5} (K)	$2.013*10^3$	__	$1.984*10^3$	__	-28.18	1.39

TABLE (4.5): IRON CHARGE WITH SINGLE BAD DATA

$S_e = 0.67531$

$S_m = 0.9486$

$S_e/S_m = 0.7119$

$J(x) = 20.6491$

Variable	True Value Z_t	Measured Value Z_m	Estimated Value Z_e	Z_m-Z_t	Z_e-Z_t	Error %
T_{s1} (K)	$3.89*10^2$	$4.006*10^2$	$4.048*10^2$	11.67	15.82	
T_{s2} (K)	$6.825*10^2$	$7.087*10^2$	$7.014*10^2$	26.22	18.9	
T_{s3} (K)	$1.080*10^3$	810.15	$1.056*10^3$	-270.05	-23.89	
T_{s4} (K)	$1.493*10^3$	$1.540*10^3$	$1.537*10^3$	47.18	43.78	
Q_l (W)	$4.729*10^3$	$4.604*10^3$	$4.648*10^3$	-124.28	-80.18	
P_t (W)	$1.41*10^5$	$1.367*10^5$	$1.372*10^5$	$-4.23*10^3$	$-3.8*10^3$	
P_{acl} (J)	$8.03*10^8$	$7.84*10^8$	$7.96*10^8$	$-1.9*10^7$	$-7.6*10^6$	
M_w (kg/s)	2.3	2.402	2.366	0.102	0.066	
T_{in} (K)	$2.98*10^2$	$3.127*10^2$	$3.12*10^2$	14.7	14.07	
T_{out} (K)	$2.985*10^2$	$3.133*10^2$	$3.129*10^2$	14.81	14.44	
T_{c1} (K)	$1.842*10^3$	__	$1.807*10^3$	__	-35.25	1.91
T_{c2} (K)	$1.864*10^3$	__	$1.824*10^3$	__	-39.68	2.13
T_{c3} (K)	$1.899*10^3$	__	$1.865*10^3$	__	-34.16	1.79
T_{c4} (K)	$1.949*10^3$	__	$1.918*10^3$	__	-30.44	1.56
T_{c5} (K)	$2.013*10^3$	__	$1.984*10^3$	__	-28.97	1.44

TABLE (4.6): IRON CHARGE WITH TWO BAD DATA
(PSEUDO MEASUREMENT FROM PRIOR INSTANT)

$S_e = 1.4857$

$S_m = 2.2471$

$S_e/S_m = 0.6619$

$J(x) = 31.4054$

Variable	True Value Z_t	Measured Value Z_m	Estimated Value Z_e	Z_m-Z_t	Z_e-Z_t	Error %
T_{s1} (K)	$3.89*10^2$	$4.006*10^2$	$3.615*10^2$	11.67	-27.64	
T_{s2} (K)	$6.825*10^2$	$7.087*10^2$	$6.462*10^2$	26.22	-36.29	
T_{s3} (K)	$1.080*10^3$	0.00	$1.028*10^3$	-83	-51.47	
T_{s4} (K)	$1.493*10^3$	0.00	$1.429*10^3$	-495.4	-63.98	
Q_l (W)	$4.729*10^3$	$4.604*10^3$	$4.589*10^3$	-124.28	-139.9	
P_t (W)	$1.41*10^5$	$1.367*10^5$	$1.356*10^5$	$-4.23*10^3$	-5350	
P_{acl} (J)	$8.03*10^8$	$7.84*10^8$	$7.62*10^8$	$-1.9*10^7$	$-4.17*10^7$	
M_w (kg/s)	2.3	2.402	2.407	0.102	0.107	
T_{in} (K)	$2.98*10^2$	$3.127*10^2$	$3.129*10^2$	14.72	14.9	
T_{out} (K)	$2.985*10^2$	$3.133*10^2$	$3.134*10^2$	14.81	14.93	
T_{c1} (K)	$1.842*10^3$	__	$1.782*10^3$	__	-60.81	3.3
T_{c2} (K)	$1.864*10^3$	__	$1.797*10^3$	__	-67.11	3.59
T_{c3} (K)	$1.899*10^3$	__	$1.838*10^3$	__	-60.98	3.21
T_{c4} (K)	$1.949*10^3$	__	$1.887*10^3$	__	-61.59	3.16
T_{c5} (K)	$2.013*10^3$	__	$1.953*10^3$	__	-59.99	2.98

TABLE (4.7): IRON CHARGE WITH TWO BAD DATA
(PSEUDO MEASUREMENT FROM NEXT NODE)

$S_e = 1.4889$

$S_m = 2.2634$

$S_e/S_m = 0.6578$

$J(x) = 31.6233$

Variable	True Value Z_t	Measured Value Z_m	Estimated Value Z_e	Z_m-Z_t	Z_e-Z_t	Error %
T_{s1} (K)	$3.89*10^2$	$4.006*10^2$	$3.605*10^2$	11.67	-28.43	
T_{s2} (K)	$6.825*10^2$	$7.087*10^2$	$6.428*10^2$	26.22	-39.67	
T_{s3} (K)	$1.080*10^3$	0.00	$1.022*10^3$	-371.48	-57.84	
T_{s4} (K)	$1.493*10^3$	0.00	$1.422*10^3$	-784.58	-71.14	
Q_l (W)	$4.729*10^3$	$4.604*10^3$	$4.587*10^3$	-124.28	-141.26	
P_t (W)	$1.41*10^5$	$1.367*10^5$	$1.355*10^5$	$-4.23*10^3$	$-5.42*10^3$	
P_{acl} (J)	$8.03*10^8$	$7.84*10^8$	$7.626*10^8$	$-1.9*10^7$	$-4.11*10^7$	
M_w (kg/s)	2.3	2.402	2.408	0.102	0.108	
T_{in} (K)	$2.98*10^2$	$3.127*10^2$	$3.129*10^2$	14.7	14.92	
T_{out} (K)	$2.985*10^2$	$3.133*10^2$	$3.135*10^2$	14.81	14.96	
T_{c1} (K)	$1.842*10^3$	__	$1.781*10^3$	__	-61.22	3.32
T_{c2} (K)	$1.864*10^3$	__	$1.796*10^3$	__	-67.54	3.62
T_{c3} (K)	$1.899*10^3$	__	$1.838*10^3$	__	-61.28	3.22
T_{c4} (K)	$1.949*10^3$	__	$1.886*10^3$	__	-62.36	3.19
T_{c5} (K)	$2.013*10^3$	__	$1.952*10^3$	__	-60.94	3.02

TABLE (4.8): IRON CHARGE WITH THREE BAD DATA

S_e = 1.76352

S_m = 2.6683

S_e/S_m = 0.66091

J(x) = 35.5375

Variable	True Value Z_t	Measured Value Z_m	Estimated Value Z_e	Z_m-Z_t	Z_e-Z_t	Error %
T_{s1} (K)	$3.89*10^2$	$4.006*10^2$	$3.552*10^2$	11.67	-33.47	
T_{s2} (K)	$6.825*10^2$	0.00	$6.362*10^2$	-281.8	-46.25	
T_{s3} (K)	$1.080*10^3$	0.00	$1.010*10^3$	-679.5	-69.45	
T_{s4} (K)	$1.493*10^3$	0.00	$1.411*10^3$	-1092.63	-82.07	
Q_l (W)	$4.729*10^3$	$4.604*10^3$	$4.576*10^3$	-124.28	-152.5	
P_t (W)	$1.41*10^5$	$1.367*10^5$	$1.354*10^5$	$-4.23*10^3$	$-5.60*10^3$	
P_{acl} (J)	$8.03*10^8$	$7.84*10^8$	$7.625*10^8$	$-1.9*10^7$	$-4.11*10^7$	
M_w (kg/s)	2.3	2.402	2.409	0.102	0.109	
T_{in} (K)	$2.98*10^2$	$3.127*10^2$	$3.130*10^2$	14.7	15.07	
T_{out} (K)	$2.985*10^2$	$3.133*10^2$	$3.136*10^2$	14.81	15.08	
T_{c1} (K)	$1.842*10^3$	__	$1.760*10^3$	__	-82.17	4.46
T_{c2} (K)	$1.864*10^3$	__	$1.774*10^3$	__	-89.66	4.81
T_{c3} (K)	$1.899*10^3$	__	$1.816*10^3$	__	-82.85	4.36
T_{c4} (K)	$1.949*10^3$	__	$1.866*10^3$	__	-83.16	4.26
T_{c5} (K)	$2.013*10^3$	__	$1.931*10^3$	__	-81.48	4.04

5.1 INTRODUCTION:

For many applications, various techniques can be used to produce an adequate system description in the form of a linear system model driven by known inputs and white Gaussian noises, with which it is possible to develop an optimal state estimator and/or controller. However, the optimality of these devices is dependent upon complete knowledge of the parameters that define the best model for system dynamics, output relations and statistical description of uncertainties. In any practical application, these quantities are known only with some uncertainty and the performance degradation that results from improperly assigned values can be severe. One would like to readjust the assumed noise strengths in the filter's internal model, based upon information obtained in real time from the measurements becoming available, so that the filter is continually "tuned" as well as possible. Such an algorithm is often termed an adaptive or self-tuning estimation algorithm. The key to adaptation will be the residual of the state estimator. Since these are the differences between actual measurements and best measurements prediction based upon the filter's internal model, consistent mismatch indicates erroneous model formulation, and particular characteristic of the mismatch can be exploited to perform the needed adaptation [6].

5.2 KALMAN FILTER:

In 1960, R.E. Kalman published his famous paper describing a recursive solution to the discrete-data linear filtering problem. Since that time, the Kalman filter has been the subject of extensive researches and applications.

The Kalman filter is a set of mathematical equations that provides an efficient computational (recursive) solution of the least-squares method. The filter is very powerful in several aspects: it supports estimations of past, present, and even future states, and it can do so even when the precise nature of the modeled system is unknown.

The Kalman filter addresses the general problem of trying to estimate the state of a discrete-time controlled process that is governed by the linear stochastic difference equation [28];

$$x_i = [\Phi]x_{i-1} + [B]u_i + w_i \quad \ldots (5.1)$$

For which the available discrete-time measurements modeled by the linear relation [28];

$$z_i = [H]x_i + v_i \quad \ldots (5.2)$$

The random variables w_i and v_i represent the process and the measurement noise respectively. They are assumed to be with normal probability distribution.

The matrix [Φ] in the difference equation (5.1) relates the state at the previous time step (*i*-1) to the state at the current step (i). The matrix [B] relates the control input *u* to the state *x*. The matrix [*H*]in the measurement equation (5.2) relates the state x_i to the measurement z_i.

If one define x_i^{*-} to be the priori state estimate at time step (i) given knowledge of the process prior to step (i), and x_i^* to be the posteriori state estimate at step (i) given measurement z_i. Now one can define a priori and a posteriori estimate errors as [28];

$$\left.\begin{aligned} e_i^- &= x_i - x_i^{*-} \\ e_i &= x_i - x_i^* \end{aligned}\right\} \quad \ldots (5.3)$$

So the priori estimate error covariance matrix is then computed by [28];

$$[P_i^-] = E[e_i^- e_i^{-T}] \quad \ldots (5.4)$$

And the posteriori estimate error covariance matrix is computed by [28];

$$[P_i] = E[e_i e_i^T] \quad \ldots (5.5)$$

In deriving the equations for the Kalman filter, one begins with the goal of finding an equation that computes a posteriori state estimate x_i^* as a linear combination of a priori estimate x_i^{*-} and a weighted difference between an actual measurement z_i and a measurement prediction ($[H]x_i^{*-}$); which is expressed as:

$$x_i^* = x_i^{*-} + [K](z_i - [H]x_i^{*-}) \quad \ldots (5.6)$$

The [K] matrix in Eq. (5.6) is chosen to be the gain or the weighting factor that minimizes the posteriori error covariance matrix; this gain is given by [28];

$$[K_i] = [P_i^-][H]^T [HP_i^- H^T + R]^{-1} \quad \ldots (5.7)$$

Where [*R*] is the measurement error covariance matrix.

And the estimate error covariance matrix is given by [28];

$$[P_i] = [I - K_i H][P_i^-] \quad \ldots (5.8)$$

The initial conditions are given by:

$$\left.\begin{aligned} x_0^* &= E[x_0] \\ P_0 &= E\{[x_0 - x_0^*][x_0 - x_0^*]^T\} \end{aligned}\right\} \quad \ldots (5.9)$$

5.3 MULTIPLE MODEL FILTERING ALGORITHM:

There are several algorithms that exist to adapt the stochastic information on-line. These are termed as adaptive Kalman filtering algorithms due to their ability to automatically adapt the filter in real time to correspond to the temporal variation of the errors involved. One such algorithm is termed Multiple Model Adaptive Estimation (MMAE).

The MMAE algorithm runs several Kalman filters in parallel each operating using different dynamic or stochastic models. The MMAE algorithm is used to select either a single ‘best’ Kalman filter solution, or the

algorithm can be used to combine the output from all the Kalman filters in a single solution [29]. This algorithm is illustrated in figure (5.1).

Let *a* denote the vector of uncertain parameters in any model described by Eq. (5.1) and (5.2), allowing them to affect any or all of [Φ], [H], and [R]. This parameter vector assumes only a finite number of values and this finite set might be the result of discretizing a continuous parameter space by selecting a set of values $\{a_1, a_2, \ldots, a_k\}$ that are dispersed throughout the region of reasonable parameter vector values.

In fact the parameter vector assumes one of the values $a_1, a_2, \ldots, a_k$ one can seek an algorithm to produce the true conditional mean and covariance of the state simultaneously with identification of the true parameter value [30].

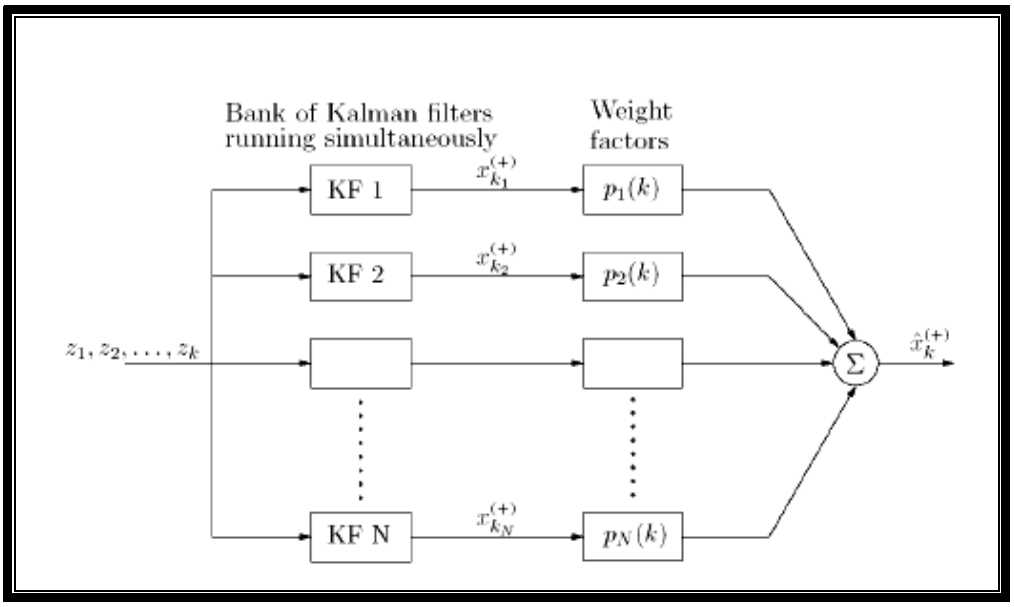

Figure (5.1): Multiple model adaptive estimation [29]

Conceptually, associated with each a_k is a different system model of the form given by Eq. (5.1) and (5.2) Thus, (*a*) is considered as a discrete random

variable, and each realization a_k corresponds to a particular model being selected by nature as the best representation of a given system. Letting $p_k(t_0)$ be the probability that (a) assumes the value a_k at time (t_0) and that $p_k(t_0)$ values must be such that [30]:

$$\left.\begin{aligned} & p_k(t_0) \geq 0 \qquad \text{for all } k, \text{ and} \\ & \sum_{k=1}^{K_f} p_k(t_0) = 1 \end{aligned}\right\} \qquad \text{... (5.10)}$$

These values reflect the one's best guess about which particular models are most likely to be correct. For example, if all models are equally likely, then $P_k(t_0) = 1 / K_f$ for all k. One can write for k=l, 2,..., K_f that [29]:

$$p_k(t_i) = \frac{f_k(z_i)\, p_k(t_{i-1})}{\sum_{j=1}^{K} f_j(z_i)\, p_j(t_{i-1})} \qquad \text{… (5.11)}$$

Where, $f_k(z_i)$ is the probability density function of the measurement z_i based on the knowledge of the parameter vector, (a), and the entire measurement history up to time t_{i-1}, or $z(t_{i-1})$. The estimated state vector at time t_i is given by [29];

$$X^*(t_i^+) = \sum_{k=1}^{K} p_k(t_i) X_k^*(t_i^+) \qquad \text{… (5.12)}$$

Where, $X^*(t_i^+)$ is the state estimate produced by a Kalman filter based on the assumption that the parameter vector equals a_k. The conditional covariance of $X(t_i)$ is [29];

$$P(t_i^+) = \sum_{k=1}^{K} p_k(t_i)\left[P_k(t_i^+) + [X_k^*(t_i^+) - X^*(t_i^+)][X_k^*(t_i^+) - X^*(t_i^+)]^T\right] \quad \ldots (5.13)$$

Where $P_k(t_i^+)$ is the state error covariance computed by the Kalman filter based on a_k. When the measurement z_i becomes available at sample time t_i, the residuals $r_1(t_i)$, $r_2(t_i)$,…, $r_k(t_i)$ are generated in the Kalman filters, and passed on for processing by the hypothesis conditional probability computation, an implementation of Eq. (5.11) specifically, each $f_k(z_i)$ could be evaluated as [29];

$$f_k(z_i) = \frac{1}{\sqrt{(2\pi)^m |A_k(t_i)|}} e^{-\frac{1}{2} r_k^T(t_i)\cdot A_k^{-1}(t_i)\cdot r_k(t_i)} \quad \ldots (5.14)$$

Where, m is the number of measurements, and $A_k(t_i)$ is generated in the k'th Kalman filter which is given by [29];

$$A_k(t_i) = H_k(t_i) P_k(t_i^-) H_k^T(t_i) + R_k(t_i) \quad \ldots (5.15)$$

If it is desired to produce an estimate of the parameter vector itself, the conditional mean of (a) at time t_i is given by [30]:

$$a^*(t_i) = \sum_{k=1}^{K} a_k p_k(t_i) \quad \ldots (5.16)$$

The residuals of the Kalman filter based upon the "correct" model will be consistently smaller than the residuals of the other mismatched filters. If this is true, then Eqs. (5.11) and (5.14) will cause the "correct" probability $p_k(t_i)$.

5.4 APPLICATION OF (MMAE) TO AN INDUCTION FURNACE:

The MMAE will be applied to the induction furnace based on figure (5.2) where the charge is made of two nodes in order to simplify and speed up of computation as compared with five nodes model used previously. Further justification is the self adaptation feature of this technique.

The heat is generated at node 2 only, some of this heat is transferred through the insulator towards node 1 and some is conducted to the inside and the remainder rise the temperature of the node itself. The heat conducted towards the center is unknown because the temperature of the next element of the charge is unknown. Thus, the heat that is used to rise the temperature of node 2 is not certain. This heat can be expressed in terms of the unknown parameter, (*a*) [6]. Therefore the system can be represented by the following set of differential equations [6]:

$$\frac{\partial T_1}{\partial t} = \dot{T}_1 = -\frac{T_1}{R_{12}C_1} + \frac{T_2}{R_{12}C_1} \qquad \ldots (5.17)$$

$$\frac{\partial T_2}{\partial t} = \dot{T}_2 = \frac{T_1}{R_{21}C_2} - aT_2 + \frac{q_2}{C_2} \quad \ldots (5.18)$$

Where R12, R21, C1, and C2 are computed as in chapter three for the two nodes model. Equations (5.17) and (5.18) can be written as:

$$\dot{T}_1 = -C_{d1}T_1 + C_{d2}T_2 \quad \ldots (5.19)$$

$$\dot{T}_2 = C_{d3}T_1 - C_{d4}T_2 + C_{d5}q_2 \quad \ldots (5.20)$$

Where,

$$C_{d1} = \frac{1}{R_{12} \cdot C_1} \quad , \quad C_{d2} = \frac{1}{R_{12} \cdot C_1} \quad ,$$

$$C_{d3} = \frac{1}{R_{12} \cdot C_2} \quad , \quad C_{d4} = a \quad , \text{ and } \quad C_{d5} = \frac{1}{C_2}$$

Equations (5.19) and (5.20) can be written in a matrix form as:

$$\begin{bmatrix} \dot{T}_1 \\ \dot{T}_2 \end{bmatrix} = \begin{bmatrix} -C_{d1} & C_{d2} \\ C_{d3} & -C_{d4} \end{bmatrix} \begin{bmatrix} T_1 \\ T_2 \end{bmatrix} + \begin{bmatrix} 0 \\ C_{d5} \end{bmatrix} q_2 \quad \ldots (5.21)$$

Now if we consider that:

$$A = \begin{bmatrix} -C_{d1} & C_{d2} \\ C_{d3} & -C_{d4} \end{bmatrix} \quad , \text{ and } B = \begin{bmatrix} 0 \\ C_{d5} \end{bmatrix}$$

Then,

$$[sI - A]^{-1} = \begin{bmatrix} s & 0 \\ 0 & s \end{bmatrix} - \begin{bmatrix} -C_{d1} & C_{d2} \\ C_{d3} & -C_{d4} \end{bmatrix} = \begin{bmatrix} s + C_{d1} & -C_{d2} \\ -C_{d3} & s + C_{d4} \end{bmatrix} \quad \ldots (5.22)$$

Where s is Laplace operator, now by taking the inverse of the above matrix one can get:

$$[sI - A]^{-1} = \frac{adj\begin{bmatrix} s + C_{d1} & -C_{d2} \\ -C_{d3} & s + C_{d4} \end{bmatrix}}{(s + C_{d1})(s + C_{d4}) - C_{d2} \cdot C_{d3}} \quad \ldots (5.23)$$

Now let,

$$(s + C_{d1})(s + C_{d4}) - C_{d2} \cdot C_{d3} = s^2 + A_c s + B_c$$

Where,

$A_c = C_{d1} + C_{d4}$, and $B_c = C_{d1} \cdot C_{d4} - C_{d2} \cdot C_{d3}$

Equation (5.23) can be written as:

$$[sI - A]^{-1} = \frac{adj\begin{bmatrix} s + C_{d1} & -C_{d2} \\ -C_{d3} & s + C_{d4} \end{bmatrix}}{(s - s_1)(s - s_2)} \quad \ldots (5.24)$$

Where,

$s_1 = \dfrac{-A_c + \sqrt{A_c^2 - 4B_c}}{2}$, and

$$s_2 = \frac{-A_c - \sqrt{A_c^2 - 4B_c}}{2}$$

Now applying the partial fraction technique to each term of Eq. (5.24) and taking the inverse Laplace transform, one can get:

$$\left.\begin{aligned} \Phi_{11} &= K_1 e^{s_1 \Delta t} + K_2 e^{s_2 \Delta t} \\ \Phi_{12} &= K_3 e^{s_1 \Delta t} + K_4 e^{s_2 \Delta t} \\ \Phi_{21} &= K_5 e^{s_1 \Delta t} + K_6 e^{s_2 \Delta t} \\ \Phi_{22} &= K_7 e^{s_1 \Delta t} + K_8 e^{s_2 \Delta t} \end{aligned}\right\} \quad \ldots (5.25)$$

Where,

$$K_1 = \frac{s_1 + C_{d4}}{s_1 - s_2} \quad , \qquad K_2 = \frac{s_2 + C_{d4}}{s_2 - s_1} \quad ,$$

$$K_3 = \frac{C_{d2}}{s_1 - s_2} \quad , \qquad K_4 = \frac{C_{d2}}{s_2 - s_1} \quad ,$$

$$K_5 = \frac{C_{d3}}{s_1 - s_2} \quad , \qquad K_6 = \frac{C_{d3}}{s_2 - s_1} \quad ,$$

$$K_7 = \frac{s_1 + C_{d1}}{s_1 - s_2} \quad , \text{ and} \qquad K_8 = \frac{s_2 + C_{d1}}{s_2 - s_1}$$

Now consider:

$$B_d(t) = \int_0^{\Delta t} \begin{bmatrix} \Phi_{11}(\Delta t - \tau) & \Phi_{12}(\Delta t - \tau) \\ \Phi_{21}(\Delta t - \tau) & \Phi_{22}(\Delta t - \tau) \end{bmatrix} \begin{bmatrix} 0 \\ C_{d5} \end{bmatrix} d\tau$$

$$= C_{d5} \int_0^{\Delta t} \begin{bmatrix} K_3 e^{s_1(\Delta t - \tau)} + K_4 e^{s_2(\Delta t - \tau)} \\ K_7 e^{s_1(\Delta t - \tau)} + K_8 e^{s_2(\Delta t - \tau)} \end{bmatrix} d\tau$$

So, the above integral becomes:

$$B_d(t) = C_{d5} \begin{bmatrix} \frac{K_3}{s_1}(e^{s_1 \Delta t} - 1) + \frac{K_4}{s_2}(e^{s_2 \Delta t} - 1) \\ \frac{K_7}{s_1}(e^{s_1 \Delta t} - 1) + \frac{K_8}{s_2}(e^{s_2 \Delta t} - 1) \end{bmatrix} \quad \ldots (5.26)$$

Therefore,

$$B_{d1} = C_{d5} \left[\frac{K_3}{s_1}(e^{s_1 \Delta t} - 1) + \frac{K_4}{s_2}(e^{s_2 \Delta t} - 1) \right] \quad \ldots (5.27)$$

$$B_{d2} = C_{d5} \left[\frac{K_7}{s_1}(e^{s_1 \Delta t} - 1) + \frac{K_8}{s_2}(e^{s_2 \Delta t} - 1) \right] \quad \ldots (5.28)$$

By making use of the above equations, then Eq. (5.17) and (5.18) can be expressed in an equivalent discrete-time model as:

$$\begin{bmatrix} T_1(t_{i+1}) \\ T_2(t_{i+1}) \end{bmatrix} = \begin{bmatrix} \Phi_{11} & \Phi_{12} \\ \Phi_{21} & \Phi_{22} \end{bmatrix} \begin{bmatrix} T_1(t_i) \\ T_2(t_i) \end{bmatrix} + \begin{bmatrix} B_{d1} \\ B_{d2} \end{bmatrix} u(t_i) \quad \ldots (5.29)$$

Now if a thermocouple is located at node 1 and measurements are taken at time interval equal to Δt, then the measurement equation is:

$$z(t_i) = \begin{bmatrix} 1 & 0 \end{bmatrix} T(t_i) + v(t_i) \quad \ldots (5.30)$$

Where $\nu(t_i)$ is the measurement noise.

In order to test the ability of the system to carry out the identification of the true parameter, the data of the furnace described in chapter one is used. For *a*= 0 and Δt= 0.1, Eq. (5.29) becomes:

$$\begin{bmatrix} T_1(t_{i+1}) \\ T_2(t_{i+1}) \end{bmatrix} = \begin{bmatrix} 1 & 4.0894*10^{-4} \\ 1.3631*10^{-4} & 1 \end{bmatrix} \begin{bmatrix} T_1(t_i) \\ T_2(t_i) \end{bmatrix} + \begin{bmatrix} 5.0654*10^{-10} \\ 2.4771*10^{-6} \end{bmatrix} q_2(t_i)$$

… (5.31)

With initial state $T_1(0)$= 323 and $T_2(0)$= 323, the filter was used to estimate T_1 and T_2. Three Kalman filters were considered with (*a*) values equal to 0, $0.5*10^{-4}$ and $1*10^{-4}$ [6]. Three cases are run holding the parameter, (*a*), constant in the " true" system equal to one of the three possible values in each case. For these cases, the filters were initialized with $X(t_0)$ set to the current T(0) values, P_0= [I], u= q_2, R= 1 and the initial hypothesis probabilities uniformly distributed, $p_k(t_0)$= 1/3.

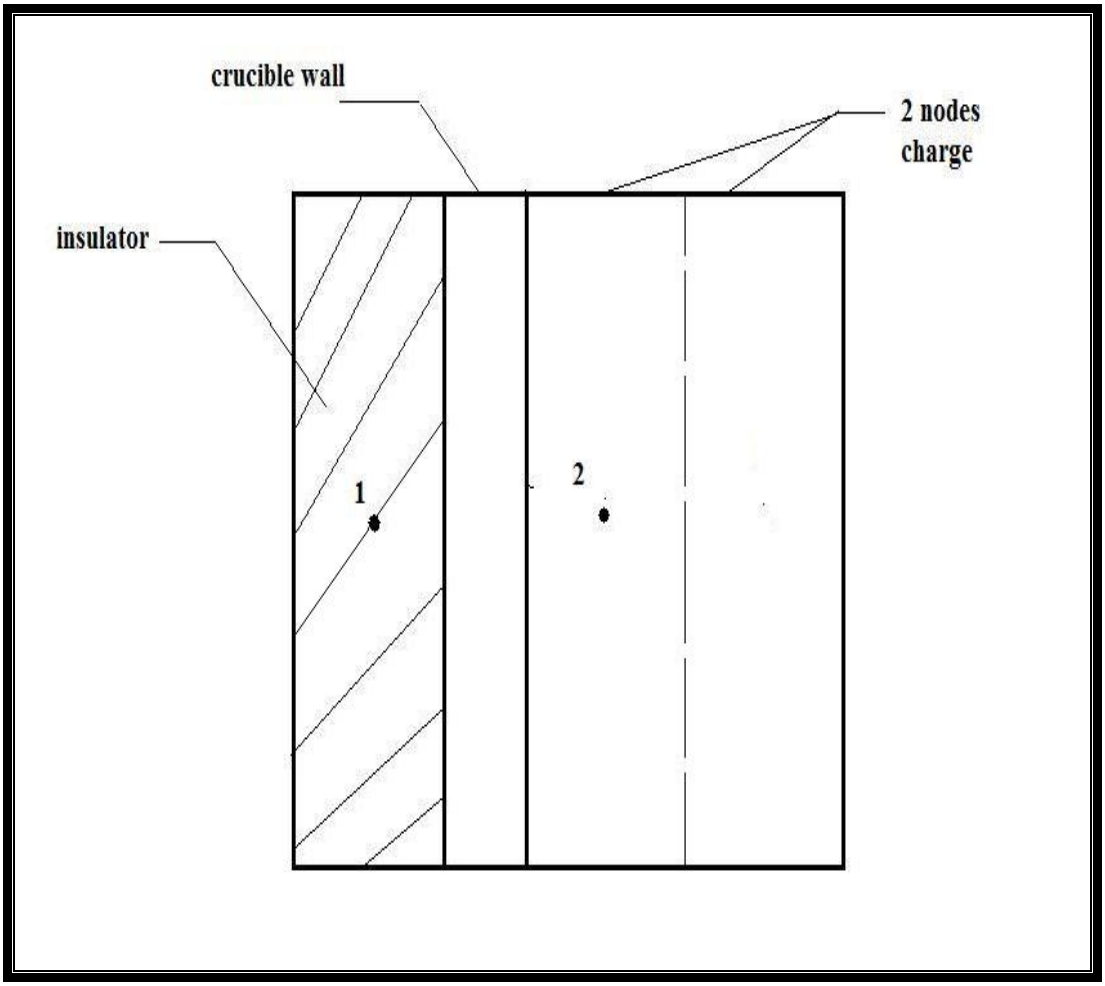

Figure (5.2): Simulation of the charge for MMAE

Figures (5.3, 4, 5) present the time histories of the conditional probabilities for all the three cases. The "true" system is always identified in less than $5*10^3$ sample periods. This illustrates the ability of the algorithm to identify constant parameters with relatively rapid convergence.

When the parameter value changes and one of these "mismatched" filters becomes the "correct" one, a transient is required to achieve proper identification. However, let the true parameter value undergo jump changes, such that $a_1 = 0$ for time interval $0 \leq t \leq 30$, $a_2 = 5*10^{-5}$ for time interval $30 \leq$

$t \leq 60$, and $a_3 = 10 * 10^{-5}$ for time interval $60 \geq t$. Figure (5.6) shows the parameter estimate provided by the algorithm.

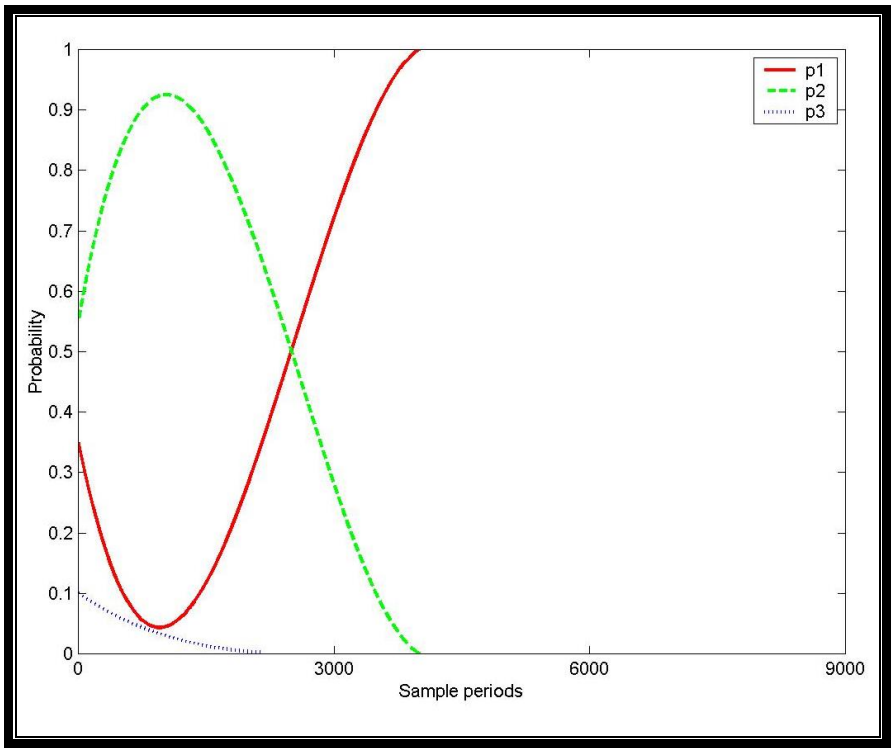

Figure (5.3): Conditional probability with true parameter value a_1

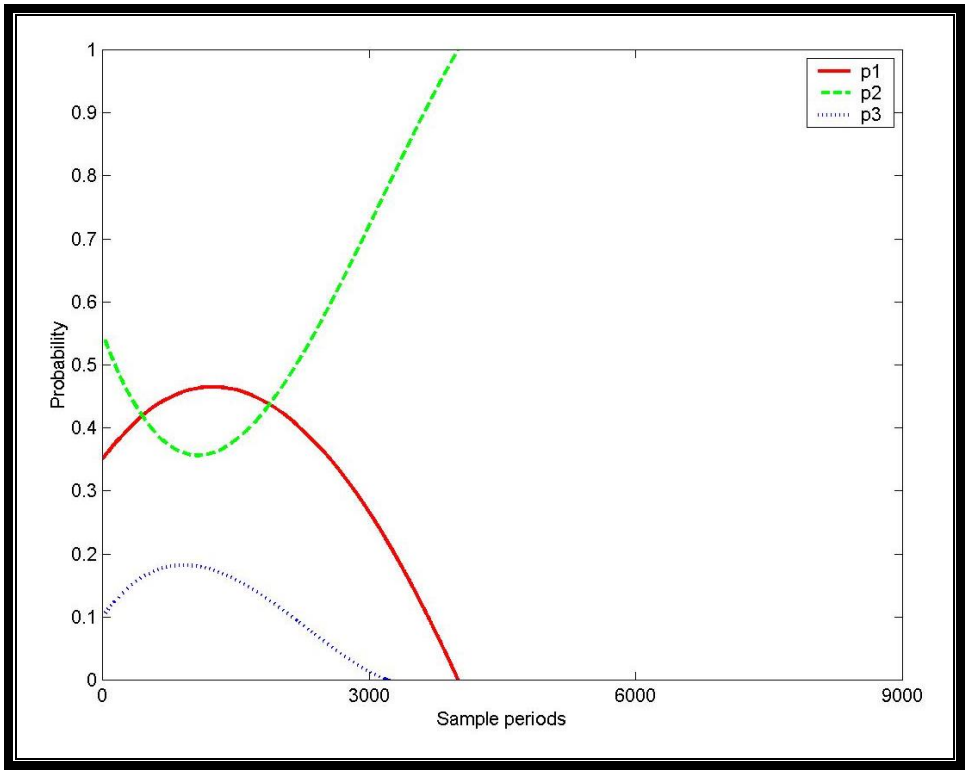

Figure (5.4): Conditional probability with true parameter value a_2

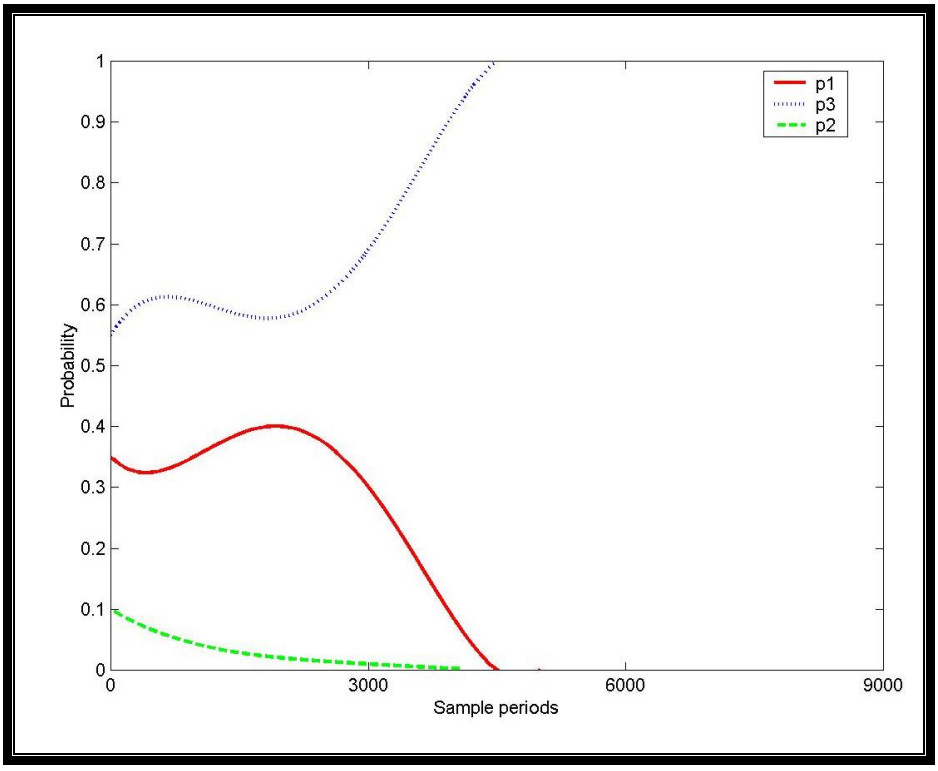

Figure (5.5): Conditional probability with true parameter value a_3

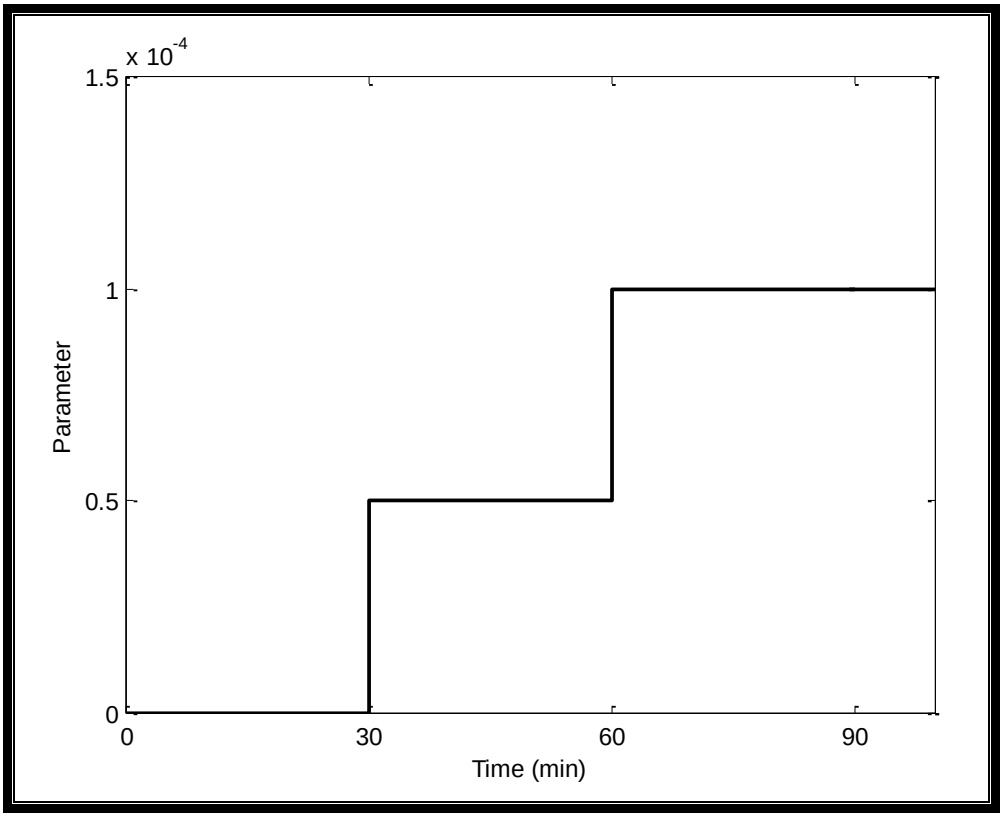

Figure (5.6): Parameter estimation using MMAE algorithm [6]

5.4.1 PERFORMANCE OF THE MMAE:

Figure (5.7) shows the estimated temperature of the iron charge of the induction furnace described in chapter one. The true value is obtained approximately from the numerical solution of the 5 nodes furnace dynamic model of chapter three.

As mentioned above the multiple model adaptive estimation MMAE algorithm depends on a 2 nodes model for the furnace charge, whereas one can use the MMAE algorithm to adapt the parameter (a) of the 2-node estimator model given by Eq. (5.17) and (5.18) to estimate the charge temperature.

The adaptation or the intelligence of this algorithm can be seen clearly, where the estimated temperature tries to follow the true value, which based on the 5 nodes model despite that the estimator model is a 2-nodes system by adjusting its parameter (*a*).

In practice, the temperature of the molten metal is bounded by its pouring temperature. This is accomplished by using a limit switch as was mentioned previously in chapter three. Figure (5.8) shows the performance of the adaptive estimator to follow the true temperature for 5-nodes model of the iron charge with a limit switch.

Figure (5.9) illustrates the ability of the estimator for estimating charge temperature for aluminum which is a paramagnetic material. In such a material the heat generation is constant, so the heating rate is constant, the conductivity is high and density is low as compared with iron. Therefore, the estimator follows the true states accurately and even faster than the case of iron. Obviously, the parameter of each Kalman filter is different than that for iron. They are 0, $0.5*10^{-5}$, and $1*10^{-5}$ for Kalman filters number 1, 2, and 3 respectively.

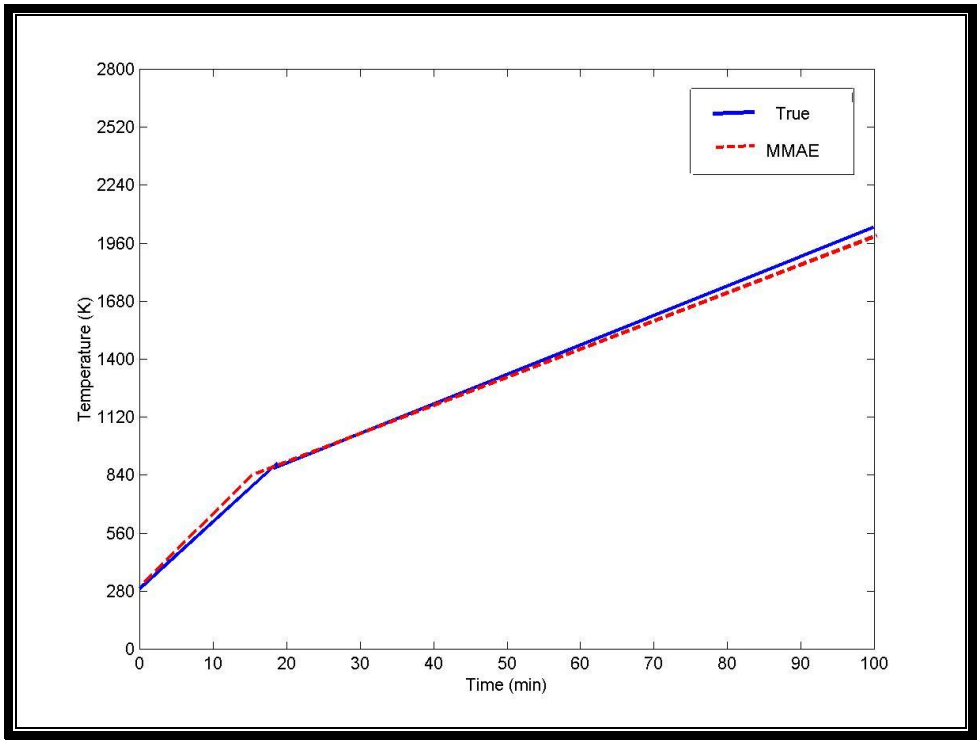

Figure (5.7): Temperature distribution with MMAE for iron charge

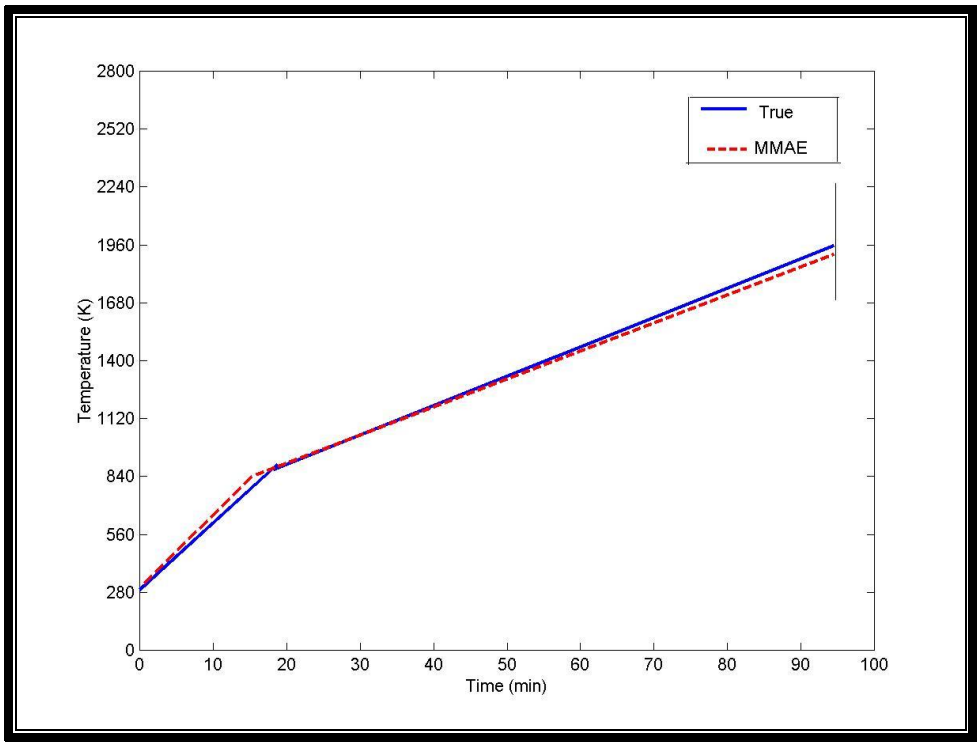

Figure (5.8): Temperature distribution with MMAE for iron charge with a limit switch

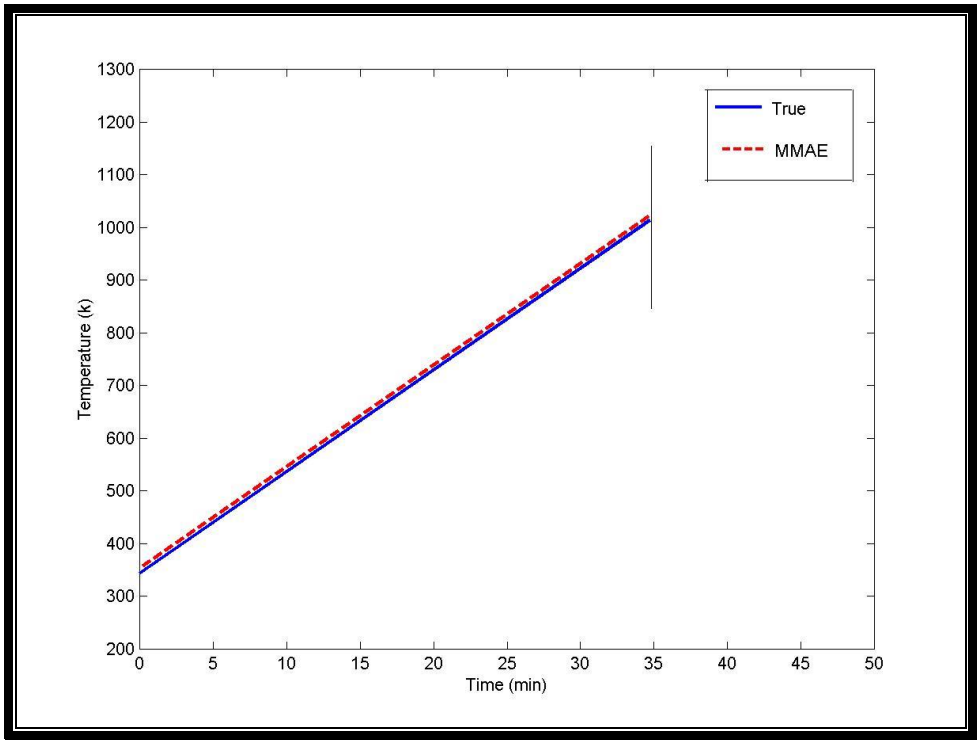

Figure (5.9): Temperature distribution with MMAE for aluminum charge with a limit switch

6.1 DISCUSSION OF SYSTEM REALIZATION:

Simulation for the furnace and the charge melting process are made in chapter three, while static and dynamic state estimation techniques are applied to induction furnace in chapters four and five. Two pure materials are tested, a ferrous material (magnetic) which is iron and a paramagnetic material which is aluminum.

1- In the furnace charge simulation, increasing the number of nodes have no effect on the results accuracy, this may be because the size of the furnace, where it is a small one (charge radius is 20 cm) so the difference between the nodes is too small.

2- In the temperature distribution of the furnace charge, figures (3, 8, 9, 10, and 11), the changing in the slope of the curves for the iron charge is due to Curie point effect on the permeability which drops to unit, where the power generation and the heating rate affected. while, in the aluminum charge the permeability is constant at unit, thus the heating rate is constant.

3- At figures (3.8, and 9), the curves of nodes (1,3) and (3,3) are close to each other while they are far-off the surface curve, this because they are primarily due to the heat conducted from the charge surface rather than by the heat generated. Same thing happened at aluminum, figures (3.10, and 11) but it does not very clear because of the high conductivity of aluminum.

4- The choice of the state vector variables are of great important where it is effect the estimator efficiency. In the present work the three element state vector proposed consists only from the elements that the operator is supplying them to the furnace which are the electrical power p_t, the cooling water temperature at the inlet of the cooling coil T_{in}, and the mass flow rate of the cooling water M_w, so all the elements of the state vector are under control.

5- Because of the state vector elements choice, present work provides exactly what the one's need or expect from the estimator which are increasing the redundancy of the measurements from 2 to 3.33 i.e., 66.5% increase. Also the error is decreased in a very noticeable values, where all the results are compared with the estimator proposed by Al-Ubaidy [6], as follows:

- The maximum node temperature error for the aluminum charge was 0.699% when the measurements suffer only from the Gaussian noise, this error is decreased with 62.15%. Also for aluminum charge the maximum error of the node temperatures raise to 1.88% when all the ten measurements have an error of one standard deviation.
- For the iron charge when the measurements have just the Gaussian noise, the charge node temperature error will be limited to 0.928%, this value raises to 2.099% when all the

measurements have an error of one standard deviation with an increase of accuracy of 81.3%.

- The estimator was tested by feeding a single bad data of 25% of the true value of the temperature of the insulator node number 3, i.e., T_{s3}, the estimator detected and identified the bad data correctly using the criteria suggested in chapter four. Even with this bad data the estimator works efficiently and estimated the charge node temperatures with a 2.13% maximum error, with an increase of accuracy of 34.88%.
- Another test for the estimator efficiency with bad data was made by feeding of two bad data which are the temperatures at nodes s_3 and s_4 of the insulator, i.e., T_{s3} and T_{s4}, where they are replaced with the measurement of the next node which is node s_2, i.e., T_{s2} as a pseudo measurement. The estimator works efficiently with maximum charge node temperature error of 3.623%, with a decrease of 69.65%.
- The estimator was tested with a very extreme condition where three bad data were fed which are the temperatures of node s_2, s_3, and s_4 i.e., T_{s2}, T_{s3}, and T_{s4}. The results showed that the estimator works efficiently with estimating the charge temperature, where even with the presence of these bad data the estimator has predicted the charge node temperatures with

maximum error of 4.81%. This error is decreased with more than 80% from its value.

6- At tables (4.6, and 7) the estimator was run with investigating the possibilities of pseudo measurements feeding, the first possibility is by feeding the pseudo measurements from the prior instant of the data history (before failure occurs), the maximum error of the charge node temperatures was 3.599%. The other possibility is by replacing the measurements of T_{s3} and T_{s4} with the measurement of the next node which is node s_2, i.e., T_{s2} as a pseudo measurement, the maximum charge node temperature error of 3.623%. This is because when the pseudo measurements are closer to the true values, the estimating results are more accuracy.

7- The estimator works with the aluminum as a paramagnetic material more efficient than with the iron. This is because the effect of the Curie point and its influence on the permeability which has a significant effect on the power generation and heating rate. Of course it will work efficient with the diamagnetic materials because the absence of the Curie point effect just like the paramagnetic materials.

8- At the start up of the furnace when transient is required before the steady state conditions are reached the dynamic state estimator works better (efficient) than the static estimator , this is because the self adapting (self tuning) of the estimation algorithm.

9- The MMAE technique used three Kalman filters to eliminate the effect of the noise in the measurement and to predict the amount of heat used to rise the temperature of node 2 of the charge (unknown parameter).

10- Figures (5.3, 4, and 5) show the probability of the true system based on the parameters a_1, a_2, and a_3 respectively, where each one of them represent the time interval that works with the value of that parameter.

11- The construction of the dynamic estimator is simpler than the static estimator because it is based on one temperature measurement in the mid-point of the insulator.

6.2 CONCLUSIONS:

1- A static state estimator for the induction furnace has been developed. Numerical tests show that the static state estimator is satisfactory for the use in state estimation.

2- The weighted least squares (WLS) approach is an effective technique in estimation, and J-index and the normalized measurements residual techniques are effective for the detection and identification process when bad data exist.

3- A better estimation of the temperature of the charge, especially at the start up of the furnace, is obtained by using the multiple model adaptive estimation (MMAE) technique as a dynamic state estimator.

6.3 RECOMMENDATIONS FOR THE FUTURE WORK:

Temperature estimation using software solution is simple, and cheap as compared with the hardware solution. Thus, attention must be paid to the application of the estimation technique which provides a solution of this problem, the following points can be recommended for the future work:

1. Using a charge with variable properties due to the temperature rise.
2. The simulation of the charge used may take into account the effect of the unoccupied volume inside the furnace.
3. New models for the static state estimation may be developed with taking into account the axial heat transfer.

CONTENTS:

EXAMINING COMMITTEE CERTIFICATE

We certify that this thesis entitled "A STUDY OF STATIC AND DYNAMIC STATE OBSERVER APPLIED TO AN INDUCTION FURNACE" and as examining committee, examined the student "HAZIM WALLY CHILLAB" in its contents and that in our opinion it meets the standard of thesis for the degree of Master of Science in Mechanical Engineering.

Signature:

Name: ***Asst. Prof. Dr. Adnan Dawood Mohammed***

(Chairman)

Date: / /2009

Signature:

Name:. ***Asst. Prof. Dr. Y. A. Faraj***

(Member)

Date: / /2009

Signature:

Name: ***Lecturer Dr. Basim A. Abass***

(Member)

Date: / /2009

Signature:

Name: ***Asst. Prof. Dr. Ahmed A. Al-Rajihy***

(Supervisor)

Date: / /2009

Signature:

Name: ***Asst. Prof. Dr. Ala M. Hosain***

(Supervisor)

Date: / /2009

Approval of the Mechanical Engineering Department
Head of the Mechanical Engineering

Signature:
Name: ***Asst. Prof. Dr. Adil A. Alwan Al- Moosawy***

Date: / /2009

Approval of the College of Engineering
Dean of the College of Engineering

Signature:
Name: ***Asst. Prof. Dr. Salah Taufiq Ali Al-Bazaz***

Date: / /2009

A_w : Work cross sectional area m^2

ber
bei
ber`
bei` } modified Bessel functions (Kelvin functions) and their derivatives

C : Effective thermal capacitance

C_p : Specific heat of the charge kJ/kg.^oK

C_{pw}: Specific heat of water kJ/kg.^oK

d_c : Diameter of the induction coil m

f : Frequency Hz

H_o: Magnetic flux intensity Weber

[H]: Jacobian matrix

I_c : Coil current A

I_r : Current density at shell of radius r A/m^2

I_{tr} : Current flowing at shell of thickness δ_r A

k_c : Thermal conductivity of charge material W/m.^oK

k_{cu} : Thermal conductivity for copper W/m.^oK

k_{ins} : Thermal conductivity for insulator material W/m.^oK

k_z : Thermal conductivity for zircon W/m.^oK

l_c : Coil length m

l_w : Work length m

M_c : Mass of the charge kg

M_w: Mass flow rate of the water kg/s

Nm : Number of the measurements

Ns : Number of the state variables

no : Number of the coil turns

P_{acl} : Equivalent heat supplied at the terminals of the coil kJ

P_w : Power generation at the surface of the charge kW

p_t : Electrical power supplied to the coil kW

Q_l : Heat escaped from the charge towards the cooling coil kW

qhc : Coil power loss kW

q_i : Power generated at a node kW

R : Effective thermal resistance

[R] : Weighted matrix

R_r : Charge resistance to I_r at shell of radius r **Ω**

r : Radius of shell in the charge m

r_c: Radius of the charge m

r_{c1}, r_{c2}, r_{c3}, r_{c4}, r_{c5} : Radii of the charge at nodes c_1-c_5 m

r_{ins} : Radius of the end of the insulator m

r_j : The measurement residual

r_l : Radius of the end of the refractory m

r_{s1}, r_{s2}, r_{s3}, r_{s4} : Radii of nodes s_1-s_4 m

r_w : Radius from center to the cooling coil m

S_e: Statistical index of the estimates

S_m : Statistical index of the measurements

T : Temperature ^oK

T_a : Temperature at adjacent node ^oK

T_c : Charge surface temperature ^oK

T_{c1}, T_{c2}, T_{c3}, T_{c4}, T_{c5} : Temperatures at nodes c_1-c_5 ^oK

T_{in} : Water temperature at cooling coil inlet ^oK

$T_{initail}$: Initial charge temperature ^oK

T_{out} : Water temperature at cooling coil outlet ^oK

T_1, T_2, T_3, T_4 : Temperatures at nodes s_1-s_4 ^oK

t : Time s

t_j : Detection threshold

t_r : Thickness of refractory lining m

u : Control input

v : Measurement noise

w : Process noise

X : State vector

x : state

y_i^{norm} : Normalized measurement residual

Z : Measurement vector

z_e : Estimated value

z_m : Measured value

z_p : Pseudo measurement

z_t : True value

Δr, Δz, $\Delta \varphi$: Geometrical parameters of the furnace

δ : Skin depth m

δ_c :	Current depth at the coil	m
δ_r :	Thickness of shell at radius r	m
θ :	Measurements noise	
μ_r :	Permeability	
ρ :	Charge density	kg/m^3
ρ_e :	Resistivity of charge material	Ω.m

Other symbols are defined as they appear in the text.

1. **Heat Treater, " Fundamental principles and applications of induction heating", Chapman & Hall Ltd., London, 1947.**
2. **John M. Svoboda, "Tech. commentary: Clean, quiet, cost-effective metals melting", Electric Power Research Institute, Inc., 1991.**
3. **Jack Wallace, and David Schwam, " overview of melting technologies", BCS Incorporated, 2005.**
4. **Polak T. A., and Pande C., " Engineering measurements methods and intrinsic errors", St. Edmunds press Ltd., 1999.**
5. **Ernest O. Doebelin, "Measurement systems applications and designs", McGraw-Hill Book Company, 3rd edition, 1983.**
6. **Al-Ubaidy M. A. J., "Charge temperature estimation of an induction furnace", M. Sc. Thesis, Al-Nahrain University, 1994.**
7. **Bala K. C., "Design analysis of an electric induction furnace for melting aluminum scrap", AU J. T., Vol. 9, No. 2, pp. 83-88, 2005.**
8. **Baker R. M., "Classical heat flow problems applied to induction billet heating", AIEE Trans., Vol. 77, pp. 106-112, 1958.**
9. **Schweppe F.C., Wildes J., and Rom D.B., "Power system static-state estimation, Parts I, II and III", IEEE Transactions on Power Apparatus and Systems, Vol. PAS-89, No. 1, pp. 120-135, 1970.**
10. **Dopazo J. F., Klitin O. A., and Van Slyck L. S., " State calculations of power system from line flow measurements", IEEE Transactions**

on Power Apparatus and Systems, Part I, Vol. PAS-89, No. 7, pp. 1698-1708, 1970, Part II, Vol. PAS-91, pp. 145-151, 1972.

11. **Lenden B., Hamza M. H., and Sheirah M. A., " Different methods for estimating thermal diffusivity of a heat process", Automatica, Vol. 12, pp. 445-456, 1976.**
12. **Lausterer G. K., Ray W. H., and Martens H. R., "Real time distributed parameter state estimation applied to a two dimensional heated ingot", Automatica, Vol. 14, pp. 335-344, 1978.**
13. **Soderstrom T., Ljung L., and Gustavsson I., "A theoretical analysis of recursive identification methods", Automatica, Vol. 14, pp. 231-244, 1978.**
14. **Tysso A., " Modeling and parameter estimation of a ship boiler", Automatica, Vol. 17, No. 1, pp. 157-166, 1981.**
15. **Xiang N., Wang S., and Yu E., " A new approach for detection and identification of multiple bad data in power system state estimation", IEEE Transactions on Power Apparatus and Systems, Vol. PAS-101, No. 2, pp. 454-462, 1982.**
16. **Mili L., Van Cutsem T.,and Ribbens-Pavella M., "Bad data identification methods in power system state estimation – A Comparative study", IEEE Transactions on Power Apparatus and Systems, Vol. PAS-104, No.11, pp. 3037-3049, 1985.**

17. **Stavros A. Argyropoulos, Osama T. Albahrana, and Renard M. Closset, " Micrpprocessor control in metallurgical furnaces", Jornal of metals, pp. 51-54, 1985.**

18. **Potapov I. N., Leibenzon A. S., Shamanaev V. I., and Sobol A. A., "Mathematical model of induction heating of solid round billet", Steel in the USSR, Vol. 16, No. 5, pp. 244-245, 1986.**

19. **Leite da Silva A. M., Do Coutto Filho M. B., and Cantera J. M. C., "An efficient dynamic state estimation algorithm including bad data processing", IEEE Transaction on Power Systems, vol PWRS-2, No. 4, pp. 1050-1058, 1987.**

20. **Jifeng Ru, and X. Rong Li, " Variable-structure multiple-model approach to fault detection, identification, and estimation", IEEE Transactions on Control Systems Technology, Vol. 16, No. 5, pp. 1029-1038, 2008.**

21. **Simpson P. G., " Induction heating coil and system design", McGraw-Hill, 1960.**

22. **Lee Howard, and Graham Freeman, " Induction heating guide", Inductoheat Banyard Publications, 2003. Available at: http://www.inductoheat.co.uk**

23. **Ben-Yaacov G. Z., and Bohn J. G., " Methodology for real time calculation of temperature rise and dynamic rating for distribution**

system duct banks", IEEE Transactions on Power Apparatus and Systems, Vol. PAS-101, No.12, pp. 4604-4610, 1985.

24. Holman J. P., " Heat transfer", McGraw-Hill, 4th edition, 1976.

25. Lo K. L., Song Z. M., Marchand E., and Pinkerton A., " Development of a static state estimator for a power station boiler, Parts I and II", Electric Power Systems research, Vol. 18, pp. 175-203, 1990.

26. Michael A. Chapman, " Adaptation And Installation of a robust state estimation package in the EEF utility", M. Sc. Thesis, Virginia Polytechnic Institute, 1999.

27. Charles H. B., and Corrinne P. B., " Understandable statistics concepts and methods", Houghton Mifflin Company, 2003.

28. Greg Welch, and Gary Bishop, " An introduction to the Kalman filter", UNC-Chapel Hill, 2001.

29. Christopher Hide, Terry Moore, and Martin Smith, " Multiple model Kalman filtering for GPS and low-cost INS integration", IESSG publications, 2005.

30. Maybeck S. Peter, " Stochastic models estimation and control", Vol. 2, Academic Press Inc., 1982.

31. Schweppe F. C., and Handschin E. J., "Static state estimation in electric power systems", Proceedings of the IEEE, Vol. 62, No. 7, 1974.

32. Mili L., Cheniae M. G., Rousseeuw P. J., "Robust state estimation of electric power systems", IEEE Transactions on Circuits and Systems, Vol. 41, pp. 349-358, 1994.

33. Xiangheng Liu, and Andrea Goldsmith, " Kalman filtering with partial observation losses", Stanford University, 2004.

34. John B. Moore, " Statistical filtering", Australian Research Committee, 1977.

35. Lee Semiatin, " Tech. commentary: Induction heating technology", Electric Power Research Institute, Inc., 1993.

36. Thakur S. S., and sinha A. K., " A robust dynamic state estimator for electric power systems", IE Journal-EL, Vol. 84, pp. 42-46, 2003.

37. Ljung L., " analysis of a general recursive prediction error identification algorithm", Automatica, Vol. 17, No. 1, pp. 89-99, 1981.

38. Omar M., and Ahmed H., " Numerical analysis", 2005. Available at: http://www.tkne.net

39. John B. Moore, " On strong consistency of least squares identification algorithms", Automatica, Vol. 14, pp. 505-509, 1978.

40. Maffezzoni C., and Marchese V., " Structural parameter estimation in power systems", Automatica, Vol. 17, No. 2, pp. 263-279, 1981.

41. Nakamura H., and Akaike H., " Statistical identification for optimal control of supercritical thermal power plants", Automatica, Vol. 17, No. 1, pp. 143-155, 1981.

42. Pieter W. Otter, " Identification and estimation of discrete state-vector models with stochastic inputs", Automatica, Vol. 17, No. 2, pp. 389-391, 1981.

43. Robert B. Asher, Kenneth D. Herring, and Jesse C. Ryles, " Bias, variance, and estimation error in reduced order filters", Automatica, Vol. 12, pp. 589-600, 1976.

44. Brewer H. W., and Leondes C. T., " A treatment of nonwhite measurement noise in discrete linear systems", Automatica, vol. 12, pp. 371-374, 1976.

45. Gerald J. Bierman, " Measurement updating using the U-D factorization", Automatica, Vol. 12, pp. 375-382, 1976.

46. Petre Stoica, and Torsten Soderstrom, " Analysis of an output error identification algorithm", Automatica, Vol. 17, No. 6, pp. 861-863, 1981.

47. Roberts P. D., and Williams T. W. C., " On an algorithm for combined system optimization and parameter estimation", Automatica, Vol. 17, No. 1, pp. 199-209, 1981.

الخلاصة:

تستخدم افران الحث بشكل واسع لصهر المعادن بمختلف انواعها وذلك لما تتمتع به من خواص تميزها عن غيرها من تقنيات التسخين والصهر. تستخدم معالجات الصهر (melting processors) لتسهيل عملية تشغيل الفرن والسيطرة عليه و مراقبته من قبل المستخدم و تعتبر عملية مراقبة وتحديد درجة حرارة الشحنة ذات اهمية كبيرة.

تم في هذا العمل الاستفادة من امكانية استخدام طريقة تخمين الحالة (state estimation) لتحديد درجة حرارة الشحنة لفرن البودقة الحثي (crucible induction furnace) ذو سعة نصف طن بالاعتماد على ما متوفر من قراءات من النظام.

مثِلت عملية الصهر باستخدام برنامج حاسوبي، وتم عمل نموذج رياضي لحالة التخمين المستقر (steady state estimation) بالاعتماد على قياس درجة حرارة بطانة الفرن (العازل) في اربعة مواقع بشكل نظري. وباستخدام هذا النموذج تم اعتماد مخمن ستاتيكي بفائض قياسات (measurement redundancy) مقداره 3.33 باستخدام طريقة مربعات الفروقات الموزونة (WLS) وتم اختباره في حالات ضوضاء عشوائية، واظهرت النتائج انه يعمل بشكل جيد حتى في حالة وجود قراءات خاطئة بفعل قصور أو فشل بعض اجهزة القياس حيث تم اختبار قدرة المخمن على التعامل مع وجود ثلاث قراءات خاطئة أي حوالي ثلث عدد القراءات و برغم ذلك فان درجة حرارة الشحنة تم تخمينها بشكل جيد و بنسبة خطأ قليلة جدا.

كما تم اعتماد طريقة اخرى لتخمين درجة حرارة الشحنة باستخدام طريقة المخمن المتكيف متعدد النموذج (MMAE) كمخمن ديناميكي بالاعتماد على مرشحات كالمن (Kalman filters) وعلى قياس درجة حرارة موقع واحد (بدلا من اربعة) داخل بطانة الفرن. اظهرت النتائج ايضا جودة المخمن و تخمينه درجة حرارة الشحنة بدقة عالية.

ABSTRACT:

Crucible induction furnaces are frequently used in melting processes with high potentials. Operation of such installation demands particular attention on the part of the operator to exploit their full potential. Melting processors are used to relief the operator and ensure proper operation of the furnace. Prediction and monitoring the charge temperature and other variables is of great importance.

The work presented in this thesis, takes advantage of the possibility of using state estimation technique in assigning a value to the temperature of the induction furnace charge as an unknown state variable based on the measurements from the furnace system according to some criteria.

A computer simulation for the melting process of the charge is developed. A mathematical model for the steady state estimation is proposed based on using four thermocouples (theoretically) located in the furnace insulation layer. Using this mathematical model, a static state observer with a measurement redundancy of 3.33 is developed using the weighted least squares (WLS) approach and it is tested in a random noise environment. Results showed that the observer is efficient and works well even when one-third of the measuring devices are failed.

Bad data detection is performed using the J-index technique. The ability of the observer to process multiple bad data is also tested and the results showed a good observer with a very good accuracy.

Finally, the multiple model adaptive estimation MMAE is applied to the furnace as a dynamic observer. This technique is based on adaptive Kalman filter using a single temperature measurement in the furnace lining (instead of four). The tested results showed a better accuracy than the static observer.